scientific reports

Check for updates

OPEN

Lamina-associated polypeptide 2α is required for intranuclear MRTF-A activity

Ekaterina Sidorenko[1], Maria Sokolova[1], Antti P. Pennanen[1], Salla Kyheröinen[1], Guido Posern[2], Roland Foisner[3] & Maria K. Vartiainen[1]✉

Myocardin-related transcription factor A (MRTF-A), a coactivator of serum response factor (SRF), regulates the expression of many cytoskeletal genes in response to cytoplasmic and nuclear actin dynamics. Here we describe a novel mechanism to regulate MRTF-A activity within the nucleus by showing that lamina-associated polypeptide 2α (Lap2α), the nucleoplasmic isoform of Lap2, is a direct binding partner of MRTF-A, and required for the efficient expression of MRTF-A/SRF target genes. Mechanistically, Lap2α is not required for MRTF-A nuclear localization, unlike most other MRTF-A regulators, but is required for efficient recruitment of MRTF-A to its target genes. This regulatory step takes place prior to MRTF-A chromatin binding, because Lap2α neither interacts with, nor specifically influences active histone marks on MRTF-A/SRF target genes. Phenotypically, Lap2α is required for serum-induced cell migration, and deregulated MRTF-A activity may also contribute to muscle and proliferation phenotypes associated with loss of Lap2α. Our studies therefore add another regulatory layer to the control of MRTF-A-SRF-mediated gene expression, and broaden the role of Lap2α in transcriptional regulation.

In eukaryotic cells, precise control of gene expression depends on the coordinated work of transcription factors and their cofactors, which also link cellular signaling events to RNA polymerase II recruitment and activation at gene promoters. Many transcription factors themselves have relatively low effector activity, and they therefore cooperate with a cofactor that has this activity[1]. One well-described example of such cooperation is serum response factor (SRF), and its cofactors, which together regulate the expression of both immediate-early and many cytoskeletal and muscle-specific genes[2,3].

Two families of signal-regulated coactivators, which interact with SRF in a competitive manner, mediate differential regulation of SRF target gene expression[4,5]. The ternary complex factor (TCF) family of proteins, regulated by the Ras-ERK signaling, mediates the immediate-early transcriptional response[6]. The myocardin-related transcription factors (MRTFs) MRTF-A (also known as MKL1 or MAL), MRTF-B, and myocardin regulate the expression of muscle-specific and cytoskeletal genes. Expression of myocardin is restricted to smooth and cardiac muscle, but both MRTF-A and MRTF-B are expressed rather ubiquitously, regulate the expression of cytoskeletal genes and respond to the Rho-actin pathway[4,7]. The subcellular localization and activity of MRTF-A (and MRTF-B) is regulated by cytoplasmic and nuclear actin dynamics, which create a feedback loop, where cytoskeletal dynamics controls the expression of its constituents[7]. In resting, unstimulated conditions, MRTF-A is mainly localized to the cytoplasm, due to the formation of a complex between monomeric actin and RPEL domain of MRTF-A. The bipartite nuclear localization signal (NLS) of MRTF-A is buried by actin-binding, which restricts import factor access, and thus prevents nuclear import of MRTF-A at high actin monomer concentrations[8–10]. In addition, actin-binding also promotes nuclear export of MRTF-A via an unknown mechanism[8,10]. Chemical or mechanical stimulation, which induce actin polymerization, for example via activation of the small GTPase RhoA, leads to dissociation of actin monomers from MRTF-A, and consequently increased nuclear import and decreased nuclear export of MRTF-A. This results in nuclear localization of MRTF-A, binding to SRF and expression of MRTF-A/SRF target genes[9,10].

Also nuclear actin dynamics contribute to MRTF-A regulation. Serum-stimulation leads to formin-dependent polymerization of actin within the nucleus, which is required for MRTF-A nuclear localization and SRF activation[11]. Subsequent study clarified the signaling events leading to nuclear actin polymerization by

[1]Institute of Biotechnology, University of Helsinki, Helsinki, Finland. [2]Institute for Physiological Chemistry, Medical Faculty, Martin Luther University Halle-Wittenberg, Halle, Germany. [3]Max Perutz Labs, Center for Medical Biochemistry, Medical University of Vienna, Vienna Biocenter Campus (VBC), Vienna, Austria. ✉email: maria.vartiainen@helsinki.fi

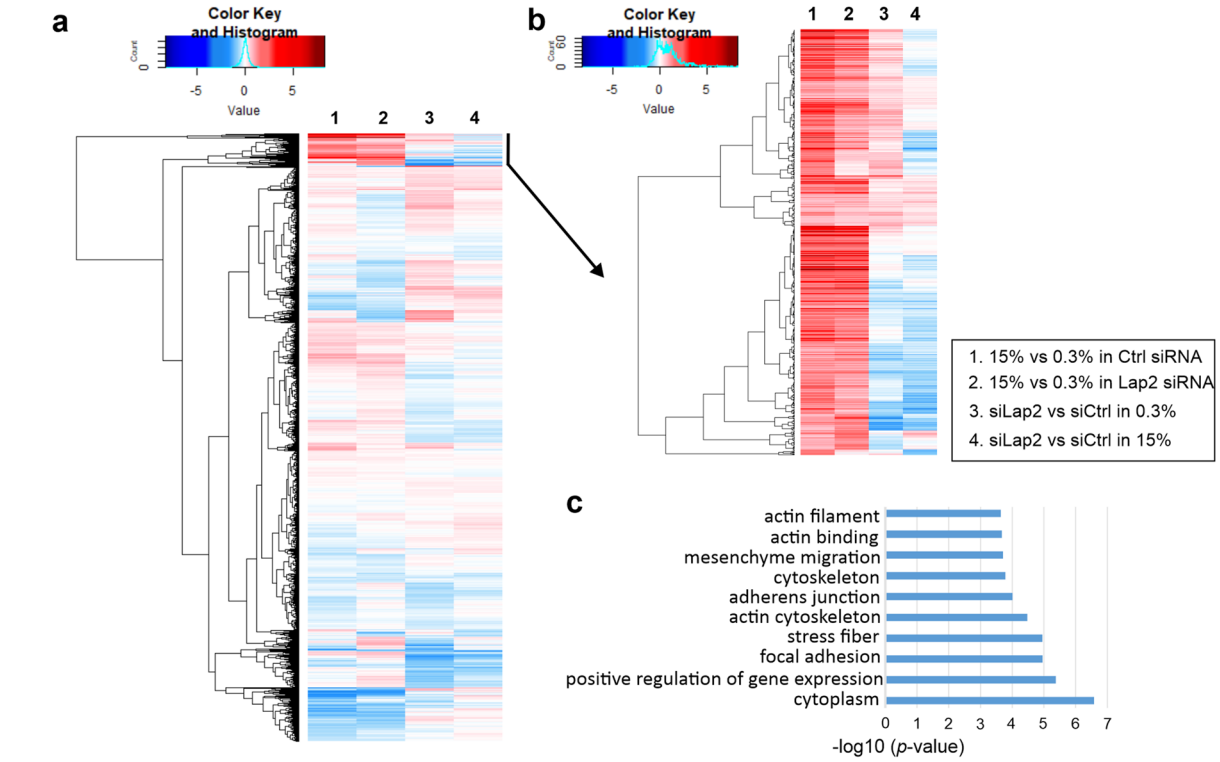
a
Color Key and Histogram
Count
Value
1 2 3 4
b
Color Key and Histogram
Count
Value
1 2 3 4
1. 15% vs 0.3% in Ctrl siRNA
2. 15% vs 0.3% in Lap2 siRNA
3. siLap2 vs siCtrl in 0.3%
4. siLap2 vs siCtrl in 15%
c
actin filament
actin binding
mesenchyme migration
cytoskeleton
adherens junction
actin cytoskeleton
stress fiber
focal adhesion
positive regulation of gene expression
cytoplasm
-log10 (p-value)

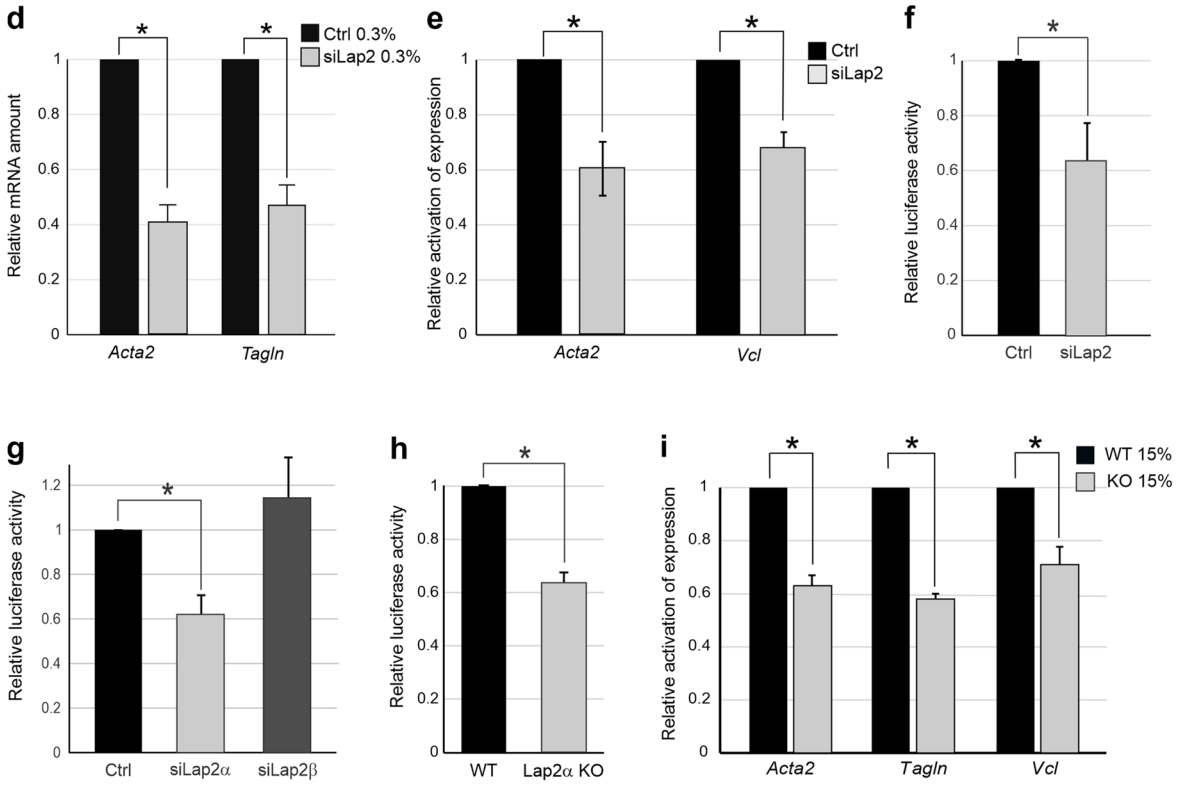
d
Relative mRNA amount
Ctrl 0.3%
siLap2 0.3%
Acta2
Tagln
e
Relative activation of expression
Ctrl
siLap2
Acta2
Vcl
f
Relative luciferase activity
Ctrl
siLap2
g
Relative luciferase activity
Ctrl
siLap2α
siLap2β
h
Relative luciferase activity
WT
Lap2α KO
i
Relative activation of expression
WT 15%
KO 15%
Acta2
Tagln
Vcl

◂**Figure 1.** Lap2α is required for MRTF-A/SRF transcriptional activity. **(a)** Heatmap showing expression of all genes in control and Lap2-depleted fibroblasts in serum-starved (0.3% serum) and serum-stimulated (15%) conditions from RNA-seq. **(b)** Heatmap showing expression of serum-responsive genes (subset of panel **a**) in control and Lap2-depleted fibroblasts in serum-starved and serum-stimulated conditions, as above. **(c)** Gene Ontology enrichment analysis of genes with decreased baseline expression or decreased activation upon serum stimulation in Lap2-depleted NIH 3T3 fibroblasts. **(d)** Depletion of total Lap2 (siLap2) decreases baseline expression (expression in serum-starved conditions) of MRTF-A target genes compared to control (Ctrl). Data is the mean with n = 5, normalized to Ctrl and error bars are standard error of the mean (s.e.m). Statistically significant differences (*; $P < 0.00001$) tested by Student's *t*-test. *P*-values: Ctrl vs siLap2 for *Acta2* 2.41×10^{-6}, Ctrl vs siLap2 for *Tagln* 9.12×10^{-5}. **(e)** Depletion of total Lap2 decreases transcriptional induction of MRTF-A target genes upon serum stimulation. Data is the mean with n = 5, normalized to Ctrl and error bars are s.e.m. Statistically significant differences (*; $P < 0.001$) tested by Student's *t*-test. *P*-values: Ctrl vs siLap2 for *Acta2* (15%FBS) 5.14×10^{-4}, Ctrl vs siLap2 for *Vcl* (15% FBS) 4.46×10^{-4}. **(f)** Depletion of Lap2 decreases serum-induced activation of a SRF reporter. Data is the mean with n = 5, normalized to Ctrl siRNA and error bars s.e.m. Statistically significant differences (*; $P < 0.01$) tested by Student's *t*-test. *P*-values: Ctrl vs siLap2 (15% FBS) 3.5×10^{-3}. **(g)** Depletion of the α-isoform (siLap2α), but not β-isoform (siLap2ß) decreases serum-induced SRF reporter activation. Data is mean with n = 4, normalized to Ctrl siRNA and error bars are s.e.m. Statistically significant differences (*; $P < 0.01$) tested by Student's *t*-test. *P*-values: Ctrl vs siLap2α 4.55×10^{-3}. **(h)** Serum-induced activation of SRF reporter activity is decreased in Lap2α KO mouse dermal fibroblasts (MDF) compared to Lap2a WT MDFs. Data is the mean with n = 7, normalized to Lap2α WT MDFs and error bars are s.e.m. Statistically significant differences (*; $P < 0.000001$) tested by Student's t-test. *P*-values: WT vs KO (15% FBS) 6.84×10^{-7}. **(i)** Serum-induced activation of MRTF-A/SRF target gene expression is decreased in Lap2α KO cells (KO) compared to Lap2α WT cells (WT). Data is the mean with n = 5, normalized to WT, and error bars are s.e.m. Statistically significant differences (*; $P < 0.001$) tested by Student's t-test. *P*-values: for *Acta2* 3.35×10^{-5}, for *Tagln:* 8.21×10^{-7}, for *Vcl* 7.19×10^{-7}. See also Supplementary Fig. 1.

demonstrating that release of Ca^{2+} from the endoplasmic reticulum targets inner nuclear membrane (INM) localized formin INF2 to promote the formation of linear actin filaments emanating from the INM[12]. Interestingly, also other proteins localized to the INM have been linked to MRTF-A/SRF regulation. Loss of lamin-A or lamin-A mutations that cause dilated cardiomyopathy-associated laminopathies result in decreased nuclear localization of MRTF-A, and impaired expression of MRTF-A/SRF target genes[13]. Mechanistically, defects in lamin A cause mislocalization of emerin, an actin-binding protein[14] from the INM to the outer nuclear membrane (ONM), which causes defects in actin dynamics[13]. In addition, emerin seems to play a critical role in the mechanical regulation of MRTF-A activity especially on stiff substrates[15]. Proteins of the linker of nucleoskeleton and cytoskeleton (LINC) complex, emerin and lamin A are also required for cell spreading-induced nuclear actin polymerization, which depends on integrin activation, and regulates the MRTF-A/SRF pathway[16]. LINC complex may also regulate MRTF-A activity by controlling the upstream signaling pathways, since Sun2-containing complexes have been demonstrated to activate RhoA and focal adhesion assembly, while Sun1 antagonizes these activities[17]. Taken together, several proteins of the nuclear envelope influence MRTF-A activity, most often by regulating actin dynamics in the cytoplasm or in the nucleus.

This study focuses on the role of lamina-associated polypeptide 2α (Lap2α) as a novel regulator of MRTF-A activity. The Lap2 family contains six alternatively spliced isoforms derived from the *Tmpo* gene[18,19]. All Lap2 isoforms share an N-terminus responsible for chromatin binding, and most of them contain a C-terminal transmembrane domain that anchors them at the INM. These anchored isoforms interact with lamin B, and help to organize heterochromatin at the nuclear periphery[20–22]. Lap2α is the largest isoform of Lap2 with a unique C-terminus lacking the transmembrane domain and expressed only in mammals[23]. Lap2α thus localizes to the nucleoplasm, where it specifically interacts with the nucleoplasmic pool of lamin A affecting lamin A properties and function[24–26]. Lap2α expression, in turn, is affected by Lamin A/C, since the absence of lamin A/C increases Lap2α protein levels[27]. Both lamin A/C and Lap2α interact with chromatin, and their binding sites overlap in euchromatic regions. Loss of Lap2α shifts lamin A/C towards more heterochromatic regions, and results in changes in epigenetic histone marks at these sites[28]. In addition to general regulation of euchromatin, Lap2α has also been linked to transcription factor regulation. It interacts with the cell-cycle regulator protein retinoblastoma (pRb) and affects E2F-pRb-dependent gene expression[29]. Indeed, loss of Lap2α leads to inefficient cell-cycle arrest, and hyperproliferation of, for example, erythroid and epidermal progenitor cells in mice[26]. Another important role of Lap2α was shown recently in human adipose-derived stem cells (hASCs), where loss of Lap2α suppresses osteogenic differentiation of hASCs via activation of NF-κB transcription factor[30]. Moreover, loss of Lap2α impairs heart function, and results in deregulation of the cardiac transcription factors GATA4 and MEF2c[31]. In addition, both Lap2β and Lap2α regulate the activity of Gli1 transcription factor by regulating its acetylation-dependent trafficking between the nuclear lamina and nucleoplasm[32]. Thus, Lap2α appears to affect the activity of different transcriptional factors in various signaling pathways.

In this work, we show that Lap2α is required for efficient MRTF-A/SRF target gene expression, and consequently for cell migration. Unlike other nuclear lamina-associated proteins implicated in this pathway, Lap2α is dispensable for MRTF-A nuclear localization. Mechanistically, Lap2α binds directly to MRTF-A and modulates MRTF-A intranuclear activity prior to chromatin binding.

Results

Lap2α is required for MRTF-A-SRF transcriptional activity. Nucleoskeletal proteins were earlier shown to affect MRTF-A nuclear localization, and hence MRTF-A activity, via modulating nuclear actin dynamics[13,16,33]. We hypothesized that also other nuclear lamina proteins might regulate MRTF-A/SRF pathway, and are here focusing on the role of lamina-associated polypeptide (Lap2) in MRTF-A/SRF regulation. To study this, we first performed siRNA-mediated knock-down of total Lap2, targeting both anchored and nucleoplasmic isoforms (Supplementary Fig. S1a), in NIH 3T3 mouse fibroblast cell line, which has been extensively used to study the MRTF-A signaling pathway[4,10,34]. To investigate the effect of Lap2 knockdown on gene expression, we performed RNA sequencing (RNA-seq) analysis of control and Lap2-depleted cells cultivated overnight in serum-starved conditions and after 45 min of serum stimulation (Fig. 1a and Supplementary Table S1.1). Serum-responsive genes responded to stimulation in both control and Lap2-depleted cells (Fig. 1a top). We identified 515 serum-inducible genes (log2FC > 1) in control samples and 521 genes that responded to stimulation (log2FC > 1) in Lap2-depleted cells (Supplementary Fig. S1b and Table S1.2). Of these genes, 356 were common for control and Lap2-depleted samples (Supplementary Fig. S1b), but they displayed weaker response to serum stimulation in Lap2-depleted cells compared to control siRNA treated cells (statistically significant differences tested by Mann–Whitney U statistical test, $P < 0.0001$) (Supplementary Fig. S1c). Serum-responsive genes clustered in two groups: the first had increased baseline expression (Fig. 1b top, column 3) and the second decreased baseline expression and decreased serum-induction (Fig. 1b bottom, columns 3, 4) in Lap2 depleted cells compared to control cells. Out of the 515 genes that were stimulated by serum in control siRNA treated cells, 110 genes displayed decreased baseline expression in starved conditions (n = 13), decreased response to serum stimulation (n = 68), or both (n = 29) (log2FC < 0.6) in Lap2-depleted cells (Supplementary Table S1.2). Gene ontology enrichment analysis of these genes revealed a number of actin cytoskeleton–related genes (Fig. 1c and Supplementary Table S1.3), strongly indicating that they likely represent MRTF-A/SRF target genes[7,35].

To confirm the recruitment of MRTF-A and SRF to serum-responsive genes, we used chromatin immunoprecipitation (ChIP) followed by deep sequencing (ChIP-seq) in serum-starved and serum-stimulated NIH 3T3 cells. Peak calling (see Materials and Methods for details) revealed that out of the 515 serum-inducible genes identified by RNA-seq, 176 genes contained peaks of either MRTF-A or SRF, or both within 100 kb from the transcription start site (TSS), indicating that many of these genes could be MRTF-A/SRF targets (Supplementary Table S1.2). Further analysis revealed increased enrichment of both SRF (Supplementary Fig. S1d-f, left) and MRTF-A (Supplementary Fig. S1d-f, right) on the SRF containing peaks upon serum stimulation (statistically significant differences tested by Mann–Whitney U test, $P < 0.00001$, Supplementary Fig. S1e*)*.

To confirm the RNA seq data, we utilized qPCR to study expression of classical MRTF-A/SRF target genes *Acta2*, *Tagln,* and *Vcl.* Depletion of Lap2 resulted in both decreased basal expression (Fig. 1d), as well as decreased transcriptional induction upon serum stimulation (Fig. 1e) of these genes. Lap2 depletion also decreased the serum-induced activation of an SRF reporter gene (Fig. 1f), further suggesting that Lap2 is a potential novel regulator of the MRTF-A/SRF transcriptional activity.

The *Tmpo* gene produces several isoforms of the Lap2 protein[18,19]. To establish which isoform is involved in regulating MRTF-A/SRF activity, we designed siRNAs targeting individually both the nucleoplasmic isoform alpha (α) (ENSMUST00000020123.6) and the anchored isoform β (ENSMUST00000072239.13) (Supplementary Fig. S1g, h). Interestingly, depletion of the Lap2α-isoform impaired the activation of the SRF reporter, whereas depletion of Lap2β-isoform had no effect (Fig. 1g).

To study this further, we took advantage of mouse dermal fibroblasts (MDF) derived from Lap2α knockout mouse[26]. As established previously, this cell line does not express any *Lap2α* mRNA[26] or Lap2α protein, whereas expression of Lap2β isoform is unaffected (Supplementary Fig. S1i). Also in this cell model, Lap2α was required for efficient MRTF-A/SRF activity, since both the SRF reporter (Fig. 1h), and MRTF-A target genes (Fig. 1i) displayed decreased serum-induced activation in Lap2α knockout (KO) cells compared to Lap2α wild type (WT) cells. These results establish Lap2α as the Lap2 isoform responsible for MRTF-A/SRF regulation.

TCFs are another set of SRF cofactors, which act as general antagonists of MRTF-dependent SRF target gene expression, competing directly with MRTFs for access to SRF[5,36]. We found that typical TCF/SRF target genes, such as *Egr1, Egr3* and *Fos* were more highly induced by serum in Lap2α KO cells than in Lap2α WT cells (Fig. 2a). Moreover, we noticed that many immediate-early genes, such as *Ctgf, Ptgs2, Cyr61, Dusp6,* and *Ier3,* were found among genes with high response to serum stimulation and increased baseline expression in Lap2-depleted cells (Supplementary Table S1.1). This result underscores the role of Lap2α in regulating specifically MRTF-A activity, and not SRF in general.

To study, if decreased MRTF-A/SRF activation also leads to any phenotypic consequences at the cellular level, we studied cell motility, because many MRTF-A target genes are responsible for cytoskeletal organization, and MRTF-A activity has been shown to be required for efficient cell migration[37–39]. Both Lap2α WT and KO cells responded to serum stimulation by increasing their motility (Fig. 2b). However, in serum-stimulated conditions, the Lap2α KO cells displayed greatly reduced migration speed compared to Lap2α WT cells (Fig. 2b). Taken together, we have established that Lap2α is a novel regulator of MRTF-A activity, and required for appropriate expression of MRTF-A target genes, which then play a critical role, for example, in cell migration.

Lap2α is not required for MRTF-A nuclear localization. One of the main mechanisms to regulate MRTF-A activity takes place via its nucleo-cytoplasmic transport, which depends on actin dynamics both in the cytoplasm and in the nucleus[10,11]. Hence, we first investigated whether Lap2α would regulate nuclear localization of MRTF-A, similarly to other components of the nuclear lamina, such as lamin A/C and emerin[13]. However, endogenous MRTF-A accumulated into the nucleus similarly in Lap2α WT and KO MDFs after 10 min or 45 min of serum stimulation (Fig. 3a, Supplementary Fig. S3a). Similarly, MRTF-A-GFP did not show any

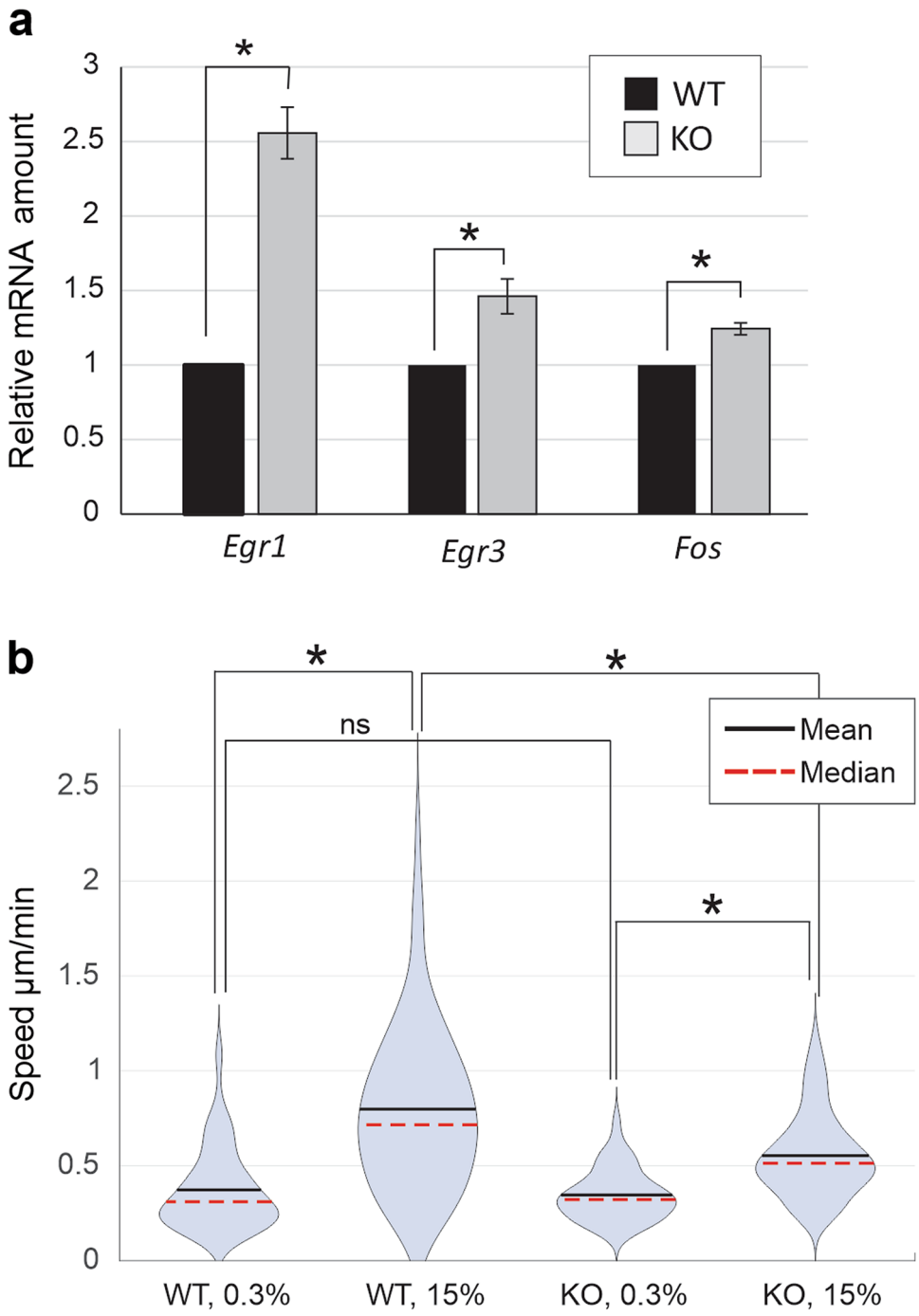

Figure 2. Loss of Lap2α leads to increased expression of TCF/SRF target genes and reduced cell migration. **(a)** Serum-induced activation of TCF/SRF target genes is increased in Lap2α KO MDFs compared to Lap2α WT MDFs. The data is shown as mean with n = 4, normalized to Lap2α WT cells and error bars are s.e.m. *Statistically significant differences ($P < 0.01$) tested by Student's *t*-test *P*-values: WT vs KO for *Egr1* 1.08×10^{-4}, WT vs KO for *Egr3* 2.5×10^{-3}, WT vs KO for *Fos* 1.45×10^{-3}. **(b)** Single cell tracking assay shows decreased motility of Lap2α KO MDFs compared to Lap2α WT MDFs in serum-stimulated conditions. Data is presented as violin plots showing distribution of average speeds for each condition with mean and median indicated. Total number of tracks: N = 89 WT 0.3%, N = 89 WT 15%; N = 107 KO 0.3%, N = 106 KO 15%. Mean values and s.t.d.: WT 0.3% 0.369 ± 0.216; WT 15% 0.783 ± 0.4; KO 0.3% 0.352 ± 0.14; KO 15% 0.556 ± 0.22. Statistically significant differences (*) tested by Kolmogorov–Smirnov test with 0.05 significance level. ns., not significant. D-values: WT 0.3% vs WT 15% 0.614; KO 0.3% vs KO 15% 0.489; WT 15% vs KO 15% 0.383; WT 0.3% vs KO 0.3% 0.174 (non-significant).

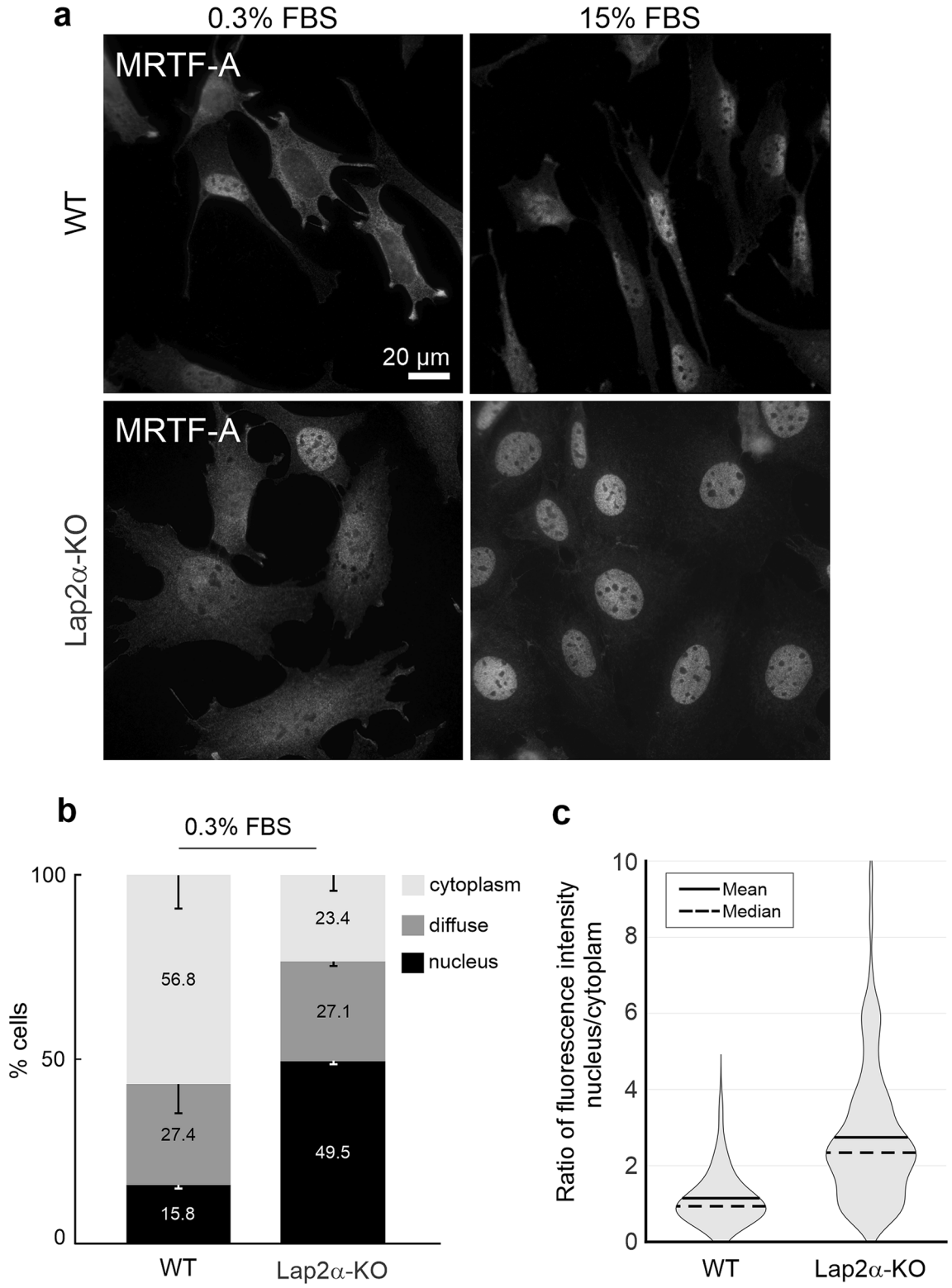

Figure 3. Lap2α is not required for MRTF-A nuclear localization. **(a)** MRTF-A localization in Lap2α WT and KO MDFs in serum starved (0.3% FBS) cells and after 10 min stimulation with 15% FBS. scale bar = 20 µm. **(b)** Quantification of MRTF-A localization in Lap2α WT and KO MDFs in serum-starved conditions (0.3%). Cells were counted in three independent experiments; total number of counted cells: for WT 395; for KO 412. Statistically significant differences (*; $P < 0.01$) tested by Student's *t*-test *P*-values: WT nucleus vs KO nucleus 2.47×10^{-4}; WT cytoplasm vs KO cytoplasm 3.57×10^{-3}. **(c)** Fluorescence intensity ratio between the nucleus and the cytoplasm for endogenous MRTF-A in WT and Lap2a KO MDF cells under starved conditions (0.3% FBS). Violin plot showing distribution of cells according to the intensity ratio (nuc/cyt). For WT: n = 117, mean = 1.147, median = 0.936, s.d. = 0.64. For KO: n = 92, mean = 2.745, median = 2.344, s.d. = 1.763. See also S3.

defects in serum-induced nuclear localization upon siRNA-mediated depletion of Lap2α in NIH 3T3 cells (Supplementary Fig. S3b). Moreover, MRTF-A nuclear localization upon Leptomycin B treatment, which inactivates Crm1/Exportin1[40], the established nuclear export receptor for MRTF-A[9,10] or upon Cytochalasin D treatment, which directly disrupts the MRTF-A-actin complex[10] was not perturbed in Lap2α KO cells (Supplementary Fig. S3 c, d). These results indicate that nuclear localization of MRTF-A is not dependent on Lap2α. To our surprise, we found that in Lap2α KO fibroblasts, MRTF-A was present in nuclei of many cells even in starved conditions (Fig. 3a–c). This indicates that unlike lamin A/C and emerin[13], Lap2α is not required for MRTF-A nuclear localization, but rather modulates its activity within the nucleus.

Lap2a is required for MRTF-A recruitment to SRF target genes. To further study the role of Lap2α in the regulation of MRTF-A activity, we examined MRTF-A-chromatin interaction in Lap2α WT and KO MDFs. We performed chromatin immunoprecipitation (ChIP) followed by deep sequencing (ChIP-seq) of MRTF-A in MDFs under serum starved (0.3% FBS) condition and 45 min after serum stimulation (15% FBS). In addition, Pol II phosphorylated at serine 5 (Pol II S5P) was included to monitor transcription activation of serum-inducible genes.

First, based on peak calling we identified the total number of MRTF-A peaks in Lap2α WT and KO cells under both conditions (Fig. 4a and Supplementary Fig. S4a**,** Supplementary Table S2). Analysis with MASC2 identified 1369 MRTF-A peaks in WT cells and 611 peaks in KO cells in serum stimulated conditions. Of these peaks, 442 were common for Lap2α WT and KO cells (Fig. 4a). As expected, in WT MDF cells, the number of MRTF-A peaks increased after serum stimulation more than two times (556 in 0.3% vs 1369 in 15% FBS). Surprisingly, in Lap2α KO MDFs, serum stimulation reduced the number of MRTF-A peaks (1004 in 0.3% vs 611 in 15% FBS). Total number of MRTF-A peaks in starved conditions was also higher in KO cells compared to WT cells (Supplementary Fig. S4a, Table S2). This may be due to increased nuclear localization of MRTF-A in KO cells compared to WT cells (Fig. 3).

We used MEME-ChIP for motif enrichment analysis and found that, as expected, the MRTF-A peaks detected in serum-stimulated conditions were significantly enriched for the SRF motif in both Lap2α WT and KO cells (Fig. 4b). Interestingly, the coverage of MRTF-A on these SRF motif-containing peaks (Supplementary Table S3.1) was much less in Lap2α KO cells than in Lap2α WT cells in serum stimulated conditions (Fig. 4c–e, Supplementary Fig. S4b). This indicates that Lap2α is required for MRTF-A recruitment to SRF target genes. According to the MEME-ChIP data analysis, MRTF-A peaks were, in addition to SRF, also enriched for motifs of several other transcription factors (TF) in both WT and Lap2α KO cells (Supplementary Table S4**).** This data indicates that MRTF-A can participate also in SRF-independent transcriptional regulation, as suggested earlier[41].

For further analysis, we located MRTF-A peaks with an SRF binding motif to the closest TSS. From 155 peaks, 59 were identified near genes with Pol II S5P coverage on the gene body at least two fold higher in serum-stimulated (15%) conditions compared to starved conditions (0.3%) in Lap2α WT cells (Supplementary Table S3.2). This group of genes included many well-established targets of the RhoA/MRTF-A/SRF pathway such as *Acta2*, *Vcl* (Fig. 4c), *Myhl9, Cap1, Myo1e,* and *Tuba1c*. For these genes, both MRTF-A binding to the SRF motif (Supplementary Fig. S4 c, d), and ratio of Pol II S5P on the gene body in serum-stimulated conditions compared to serum-starved (Supplementary Fig. S4 e, f), were decreased in Lap2α KO cells compared to Lap2α WT cells, corroborating the decreased expression of these genes in Lap2α KO cells as measured by RT-qPCR (Fig. 1i).

Thus far, our data indicates that Lap2α is required for efficient binding of MRTF-A to MRTF-A/SRF target genes, and consequently needed for their expression. Since Lap2α can also interact with chromatin, and has been shown to bind especially euchromatic regions[28], we next tested whether Lap2α would also interact with MRTF-A/SRF target genes. However, our ChIP-seq analysis failed to detect any enrichment of Lap2α on MRTF-A peaks either in Lap2a WT or in KO cells (Fig. 5a,b), strongly suggesting that Lap2α does not regulate MRTF-A activity at the promoter level. Indeed, previous studies have indicated that Lap2α, in complex with nucleoplasmic Lamin A/C, may be involved in the establishment of euchromatin environment via epigenetic mechanisms rather than regulating gene expression by directly binding to promoters[28]. To study if Lap2α modulates the epigenetic landscape of also MRTF-A/SRF target genes, we analyzed the levels of the active H3K4me3 and H3K9Ac histone marks on the promoter region of genes with the MRTF-A peaks (Fig. 5c–f, Supplementary Table S3.2**,** see also Supplementary Fig. S4c–f for Pol II S5 and MRTF-A enrichment on these genes), and on all expressed genes in Lap2α WT and KO cells (Supplementary Fig. S5a,b; ChIP-seq data from[28]). Although the MRTF-A/SRF target genes displayed decreased amount of RNA Pol II S5P in Lap2α KO cells compared to WT cells (Supplementary Fig. S4 e–f**),** the levels of H3K4me3 and H3K9Ac were very similar in both cell lines (Fig. 5c–f). In contrast, genes that were previously shown to display altered expression in Lap2α KO cells displayed increased and decreased levels of H3K4me3 and H3K9Ac histone marks on up-regulated and down-regulated genes, respectively (Supplementary Fig. S5c-f: data from[28]). Although H3K9Ac levels on the selected 59 genes appeared slightly higher in Lap2α WT than in Lap2α KO cells (Fig. 5e,f), the same difference remained for all expressed genes (Supplementary Fig. S5b), indicating that it was not a specific characteristic of MRTF-A/SRF target genes. Taken together, Lap2α does not show any preferential binding to MRTF-A/SRF target genes, and therefore the influence on H3K4me3 and H3K9Ac on these genes does not extend beyond the overall effect that Lap2α has on these histone marks.

MRTF-A binds to Lap2α. Our data so far has demonstrated that Lap2α is required for the proper recruitment of MRTF-A to its target genes. To explore the mechanism of this regulation, we hypothesized that Lap2α might interact with MRTF-A, and thus affect its activity. To study this, we performed co-immunoprecipitation (co-IP) studies in NIH 3T3 fibroblasts. First, the interaction between full-length proteins was confirmed. Antibody against tagged MRTF-A efficiently precipitated endogenous and tagged Lap2α (Fig. 6a,b, Table 1) and

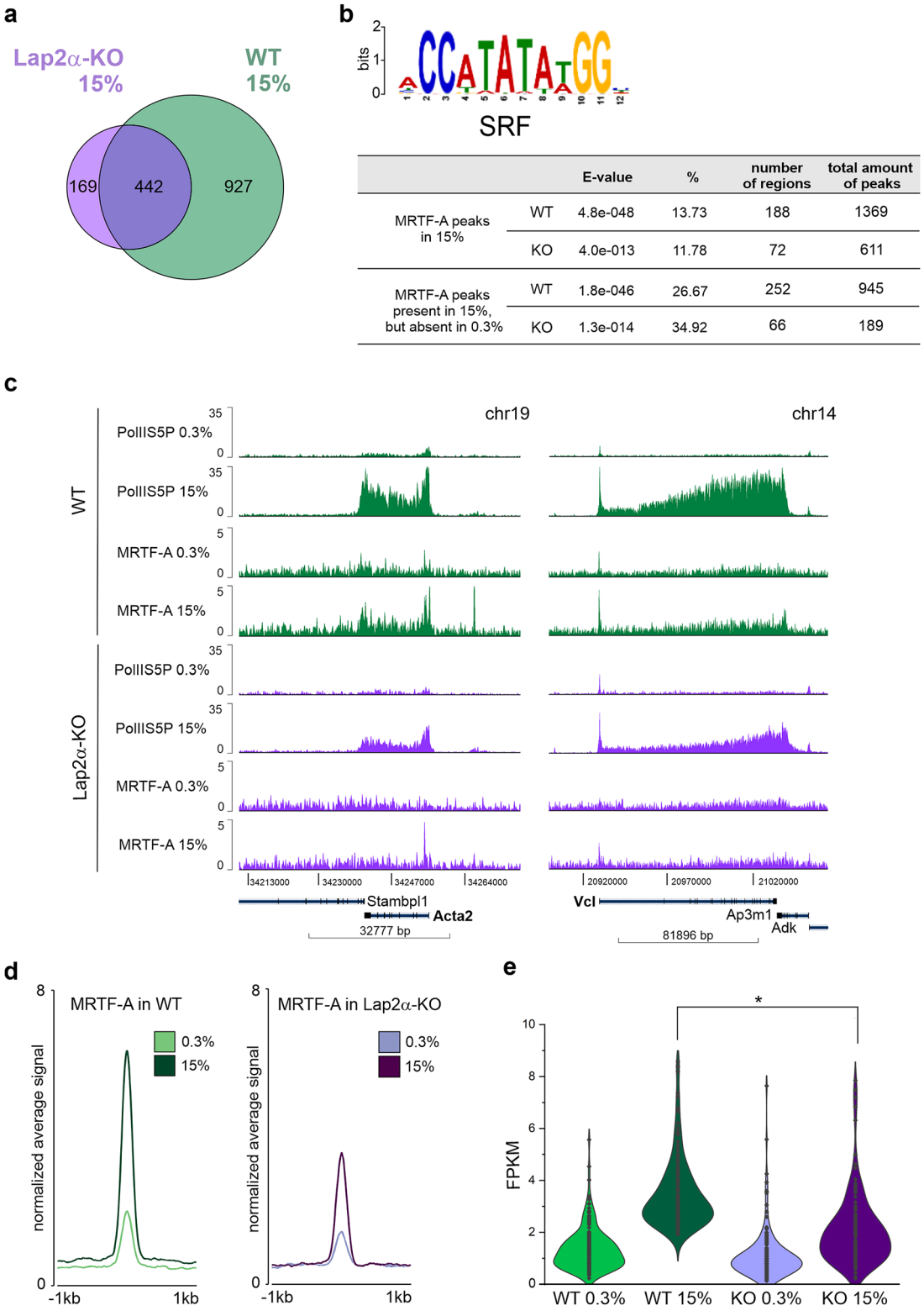

		E-value	%	number of regions	total amount of peaks
MRTF-A peaks in 15%	WT	4.8e-048	13.73	188	1369
	KO	4.0e-013	11.78	72	611
MRTF-A peaks present in 15%, but absent in 0.3%	WT	1.8e-046	26.67	252	945
	KO	1.3e-014	34.92	66	189

Figure 4. Lap2α is required for MRTF-A recruitment to SRF target genes. **(a)** Venn diagram showing overlap of MRTF-A peaks in WT and Lap2α KO cells under serum-stimulated (15%) conditions from chromatin immunoprecipitation followed by deep-sequencing (ChIP-seq). **(b)** MEME-ChIP analysis identifies SRF motif (upper part) within the MRTF-A peaks found in 15% FBS (upper table) and peaks present in 15% FBS but absent in 0.3% FBS (lower table). **(c)** Normalized (FPKM) coverage of Pol II S5P and MRTF-A on MRTF-A target genes *Acta2* and *Vcl* in Lap2α WT and KO MDFs in serum-starved (0.3%) and stimulated (15%) conditions. **(d)** Coverage of MRTF-A on the peaks with SRF motif in Lap2α WT vs KO cells in serum-starved (0.3%) and serum-stimulated (15%) conditions. Metaprofiles with average normalized fragment counts are centered on peak summits of MRTF-A in Lap2α WT in 15%. **(e)** Violin plots showing distribution of MRTF-A average normalized read counts (FPKM) at identified SRF binding sites in 15% (N = 155) at 400 bp in Lap2α WT vs KO cells in serum-starved (0.3%) and serum-stimulated (15%) conditions. Statistically significant differences (*) tested by Mann–Whitney U test $P < 0.00001$. See also Supplementary S4.

tagged Lap2α precipitated tagged full-length MRTF-A (Fig. 6c). However, we did not detect any interaction between Lap2α and SRF in similar co-immunoprecipitation experiments (Supplementary Fig. S6a), further confirming our results that Lap2α is specifically involved in regulating MRTF-A, and not SRF in general (Fig. 2a).

Next, we utilized different deletion constructs of MRTF-A to identify the functional domain (Fig. 6d, Supplementary Fig. S6b) responsible for the Lap2α interaction. First, we tested a construct consisting of the N-terminal RPEL domain of MRTF-A (Fig. 6d, Supplementary Fig. S6b), which is responsible for actin-binding and involved in MRTF-A nuclear import[9,42]. However, no interaction was detected (Fig. 6e), which goes in line with the experiments showing that Lap2α does not regulate MRTF-A nuclear import (Fig. 3). Also MRTF-A-ΔN (Fig. 6d, Supplementary Fig. S6b), which lacks the N-terminus including the RPEL domain, efficiently co-precipitated Lap2α, further confirming that Lap2α binding takes place beyond the RPEL domain (Fig. 6f). Another MRTF-A deletion construct without C-terminus (MRTF-A C471) also bound to Lap2α (Fig. 6f). Further experiments with other MRTF-A deletion constructs indicated that while the B1 domain (responsible for the SRF binding), leucine zipper (LZ) and Q domains were not required for efficient Lap2α interaction, the construct with deletion of the SAP domain (ΔSAP) showed greatly reduced interaction with Lap2α (Fig. 6g,h). Because deletion of the whole domain might disrupt protein structure and thus affect its binding ability, we introduced point mutations inside the SAP domain (see Materials and methods for details). Similarly to the deletion of the SAP domain, also these point mutations impaired the interaction between MRTF-A and Lap2α (Fig. 6i), confirming the role of the MRTF-A SAP domain in Lap2α binding. Next, we utilized C-terminal truncations of Lap2α (Fig. 6d, Supplementary Fig. S6b) to delineate the MRTF-A binding site. Unfortunately, N-terminal truncations of Lap2α were not expressed sufficiently for co-IP experiments, as has been reported also earlier[43]. Nevertheless, Lap2α constructs with deletions of the C-terminus (1–615, 1–414, 1–254) displayed similar expression levels to the full-length protein but did not show any interaction with MRTF-A (Fig. 6j). These results demonstrate that MRTF-A and Lap2α interact in cells, and that this interaction takes place via SAP-domain of MRTF-A, and requires an intact C-terminus of Lap2α.

To study whether MRTF-A binds directly to Lap2α, we performed a pull-down assay with MRTF-A expressed and purified from insect cells, and recombinant His-GST-tagged C-terminal domain (CTD) of Lap2α (Fig. 6d, Supplementary Fig. S6b) expressed in bacterial cells. MRTF-A was detected on beads coated with Lap2α-CTD, but not on beads with GST (Fig. 6k), demonstrating the direct interaction between MRTF-A and C-terminus of Lap2α. This result also supported our Co-IP data about the role of Lap2α C-terminus in the interaction with MRTF-A.

Discussion

The nucleoskeleton—a "dynamic network of networks"—provides not only mechanical support to the nucleus but contributes significantly to many nuclear activities, such as expression of specific sets of genes[44,45]. Previous studies have demonstrated that many components of the nucleoskeleton, especially nuclear actin and several components of the nuclear lamina, such lamin A/C, emerin and the LINC complex[11,13,15], regulate the activity of MRTF-A, a transcription coactivator of SRF. Here we extend these studies by showing that Lap2α, the nucleoplasmic isoform of Lap2, is a novel regulator, and a direct binding partner, of MRTF-A, and required for the expression of MRTF-A-SRF target genes by modulating MRTF-A chromatin binding. Our studies therefore add another regulatory layer to the control of MRTF-A-SRF-mediated gene expression, and broaden the role of Lap2α in transcriptional regulation.

The *Tmpo* gene produces Lap2 proteins with very different functional properties. The anchored isoforms, including the Lap2β isoform, contain transmembrane domains, and are therefore important components of the nuclear envelope, interact with lamin B and help to organize heterochromatin at the nuclear periphery[18,22]. In terms of gene expression, these anchored isoforms are mostly involved in gene silencing. For example, Lap2β has been shown to influence repressive epigenetic modifications via interaction with HDAC3, and to reduce transcriptional activity of the E2F-DP complex[46,47]. In contrast, Lap2α lacks the transmembrane domain and localizes to the nucleoplasm, where it associates with euchromatin[28]. Our experiments with siRNAs targeting specifically the anchored and nucleoplasmic isoforms of Lap2 (Supplementary Fig. S1g,h), as well as studies with the Lap2α KO cells, clearly demonstrate that Lap2α is required for MRTF-A-SRF activity, whereas the anchored isoforms are dispensable (Fig. 1g). Further studies utilizing the MDF cell line derived from Lap2α KO mice[26] confirmed the importance of Lap2α for MRTF-A/SRF function (Fig. 1h,i). The specificity of Lap2α isoform in regulating MRTF-A is also supported by our binding experiments, which showed that an intact C-terminus, which is unique to Lap2α, is required for binding to MRTF-A (Fig. 6j,k).

One of the main mechanisms to control MRTF-A activity is via its nucleo-cytoplasmic shuttling, which is regulated by both cytoplasmic and nuclear actin dynamics[10,11]. Indeed, several nucleoskeletal proteins including lamin A/C and emerin have been shown to regulate MRTF-A activity by affecting its nuclear accumulation. These proteins are required for the proper polymerization of nuclear actin, and consequently for MRTF-A activation[13,16]. However, we did not observe any defect in MRTF-A nuclear localization in Lap2α KO cells, or upon siRNA-mediated silencing of Lap2α, in any conditions that induce MRTF-A nuclear accumulation (Fig. 3a; Supplementary Fig. S3b–d). Interestingly, in Lap2α KO cells, many cells contained MRTF-A in the nucleus already in starved conditions (Fig. 3b). This could reflect activation of a feedback loop, where defective expression of many cytoskeletal genes leads to imbalance in actin polymerization, and consequently to nuclear localization of MRTF-A to correct the transcriptional defects.

The mechanism by which Lap2α impinges on MRTF-A activity is therefore different than the other nucleoskeletal proteins utilize. The fact that in Lap2α KO cells MRTF-A can localize to the nucleus (Fig. 3a), but target gene expression is impaired (Fig. 1i), implies that the regulation impinges on nuclear MRTF-A. Indeed, ChIP-seq studies revealed reduced binding of MRTF-A to SRF target genes in Lap2α KO cells (Fig. 4c,d). Also Lap2α is a

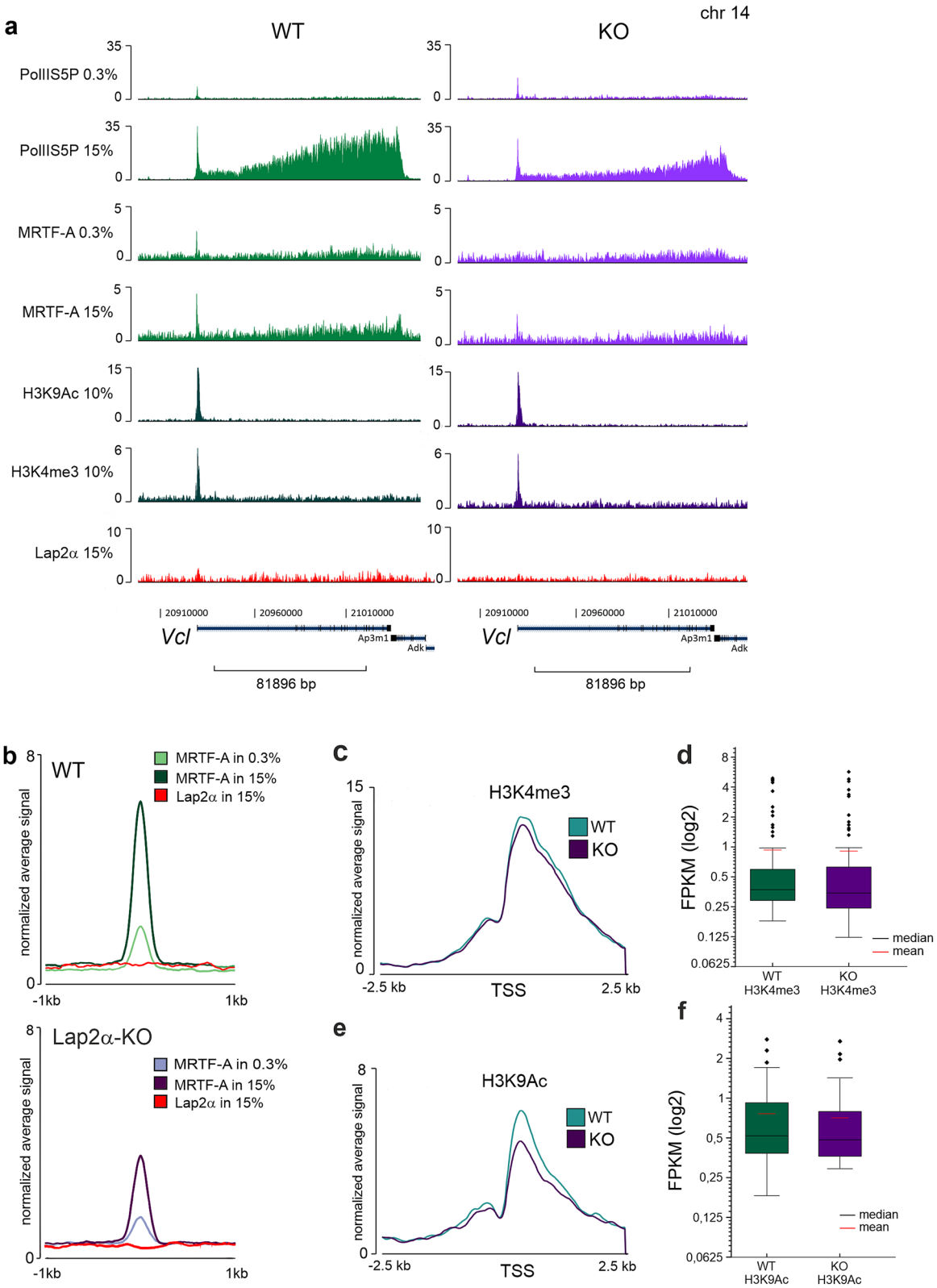
a
chr 14
WT
KO
PolIIS5P 0.3%
PolIIS5P 15%
MRTF-A 0.3%
MRTF-A 15%
H3K9Ac 10%
H3K4me3 10%
Lap2α 15%
35
5
15
6
10
0
| 20910000
| 20960000
| 21010000
Vcl
Ap3m1
Adk
81896 bp
b
WT
MRTF-A in 0.3%
MRTF-A in 15%
Lap2α in 15%
normalized average signal
8
-1kb
1kb
Lap2α-KO
c
H3K4me3
WT
KO
15
-2.5 kb
TSS
2.5 kb
d
FPKM (log2)
8
4
2
1
0.5
0.25
0.125
0.0625
median
mean
WT
H3K4me3
KO
H3K4me3
e
H3K9Ac
f
0,5
0,25
0,125
0,0625
WT
H3K9Ac
KO
H3K9Ac

◂**Figure 5.** Lap2α neither interacts with MRTF-A/SRF target genes nor modulates their active histone marks. **(a)** Normalized (FPKM) coverage of Pol II S5P, MRTF-A, H3K9Ac, H3K4me3 and Lap2α by ChIP-seq to MRTF-A target gene *Vcl* in Lap2α WT and KO fibroblasts under serum starved (0.3%) and serum stimulated (15%) conditions. Data for H3K9Ac and H3K4me3 binding were used from Gesson et al., 2016. **(b)** Coverage of Lap2α and MRTF-A on MRTF-A peaks with SRF motif in Lap2α WT and KO MDFs cells in serum-starved (0.3%) and serum-stimulated (15%) conditions. Metaprofiles with average normalized fragment counts (FPKM) are centered on MRTF-A in 15% peak summits. **(c)** Histone H3K4me3 at the TSS of 59 selected genes in WT and KO MDF. Metaprofiles show 5 kb window with average normalized fragment counts centered on TSS. **(d)** Normalized read counts (FPKM) for histone H3K4me3 at the TSS of 59 selected genes do not show significant difference between WT and Lap2α KO MDF. **(e)** Histone H3K9Ac at the TSS of 59 selected genes in WT and KO MDF. Metaprofiles show 5 kb window with average normalized fragment counts centered on TSS. **(f)** Normalized read counts (FPKM) for histone H3K9Ac at the TSS of 59 selected genes do not show significant difference between WT and KO MDF. See also Supplementary S5.

chromatin-binding protein, containing LEM and LEM-like domains at the N-terminus, which mediate chromatin binding via Barrier-to-Autointegration Factor (BANF1) and by directly binding to DNA, respectively[43,48–50]. In addition, the C-terminal region of Lap2α associates even with mitotic chromosomes[51]. Furthermore, genome-wide binding studies have indicated that Lap2α associates, together with A-type lamins, with large euchromatic regions[28]. However, we failed to detect any clear overlap between MRTF-A and Lap2α enrichment on MRTF-A/SRF target genes (Fig. 5a,b), indicating that Lap2α and MRTF-A are not interacting with target gene promoters as a complex.

The exact mechanism by which Lap2α regulates MRTF-A activity awaits further studies. One putative mechanism could be via regulation of the epigenetic landscape of MRTF-A/SRF target genes. Indeed, previous studies had reported altered levels of active histone marks H3K9Ac and H3K4me3 on genes that displayed differential expression in Lap2α KO cells[28] (Supplementary Fig. S5c–f). However, at least these histone marks were not specifically altered on MRTF-A/SRF target genes, when compared to all transcribed genes (Fig. 5c–f), further highlighting the inability of Lap2α to enrich at MRTF-A/SRF target genes. However, we cannot exclude the possibility that these minor changes in H3K9Ac and H3K4me3, or in other Lap2α-dependent histone modifications, or other Lap2α-mediated effects on chromatin environment could influence the ability of MRTF-A to bind to its target genes. Mainly in vitro studies have shown that MRTF-A/SRF interaction is favored at sites, where the DNA is easily bent[5]. Perhaps this property makes MRTF-A exquisitely sensitive to the chromatin environment, whereas the TCF/SRF interaction, occurring preferentially on a defined Ets-motif[52], would be less sensitive. Nevertheless, since our co-immunoprecipitation and pull-down experiments demonstrate a physical interaction between Lap2α and MRTF-A, but not SRF (Fig. 6a–c,k; Supplementary Fig. S6a), we favor a model, where Lap2α regulates MRTF-A activity prior to chromatin-binding. This could take place via post-translational regulation of MRTF-A. For example, MRTF-A is phosphorylated on multiple residues, and phosphorylation both positively and negatively regulates MRTF-A activity[53]. On the other hand, UBC9-mediated SUMOylation of MRTF-A reduces its transcriptional activity[54]. Another potentially interesting post-translational modification in this context is acetylation, since recent studies have shown that it can both positively and negatively influence MRTF-A activity. SIRT1-mediated deacetylation enhances the transcriptional activity of MRTF-A, and promotes its recruitment to the collagen type I promoters[55]. However, in monocytes, acetylation by PCAF promotes nuclear translocation of MRTF-A and consequent interaction with transcription factor NF-κB, thus affecting pro-inflammatory transcription[56]. MRTF-A also interacts with HDAC6, and its inhibition causes increased acetylation and levels of MRTF-A, leading to enhanced transcriptional activity of SRF. Since HDAC6 is a cytoplasmic protein, this regulation likely takes place prior to MRTF-A nuclear accumulation[57]. On the other hand, Lap2 isoforms have been shown, through competitive interactions, to regulate the activity of Hedgehog transcription factor Gli1 by controlling its acetylation, and thereby its movement between the nuclear lamina and nucleoplasm. The nuclear membrane anchored Lap2β maintains a reserve of Gli1 at the INM in acetylation-dependent manner, while Lap2α, promoted by aPKC, scaffolds Gli1 to HDAC1 for deacetylation and release from the INM[32]. In the future, it will be interesting to study, whether the direct interaction between MRTF-A and Lap2α facilitates MRTF-A activity via control of its acetylation. Further studies on the biochemical basis of MRTF-A-Lap2α interaction are needed to design e.g., rescue experiments to test these ideas.

Decreased MRTF-A/SRF activity upon lack of Lap2α revealed interesting aspects and possibilities into both MRTF-A function and phenotypical effects of Lap2α. In line with the literature describing the competitive interactions between MRTFs and TCFs for regulating SRF-mediated transcription[5], we observed increased activation of several canonical TCF target genes, such as *Egr1, Egr3* and *Fos* in Lap2α KO cells compared to Lap2α WT cells (Fig. 2a). We thus propose that the absence of Lap2α shifts the balance between MRTF and TCF-dependent gene expression towards TCFs, promoting a proliferative program. This could therefore contribute, together with the regulation of pRb, to the hyperproliferative phenotype observed upon loss of Lap2α in many contexts[26,29]. Analysis of Lap2α-deficient mice have also revealed phenotypes associated with both skeletal and heart muscle function. Loss of Lap2α leads to an increase in myofiber-associated stem cell pool and shifts the myofiber-type ratio towards fast fiber types[58]. Moreover, loss of Lap2α leads to systolic dysfunction in younger mice, as well as increased susceptibility for fibrosis in old mice. These defects in heart function are accompanied by deregulation of GATA4 and Mef2c transcription factors[31]. It is tempting to speculate that the novel function described here for Lap2α in MRTF-A regulation might play a role in muscle tissues as well. Indeed, many MRTF-A/SRF target genes are muscle-specific genes[7,59,60] and MRTFs in general are considered as important transcription cofactors for both the development of the cardiovascular system and its adaptation to injury and stress[61]. MRTF-A is also required for skeletal muscle differentiation both in vivo and in vitro[60,62]. MRTF-A is tightly regulated in skeletal

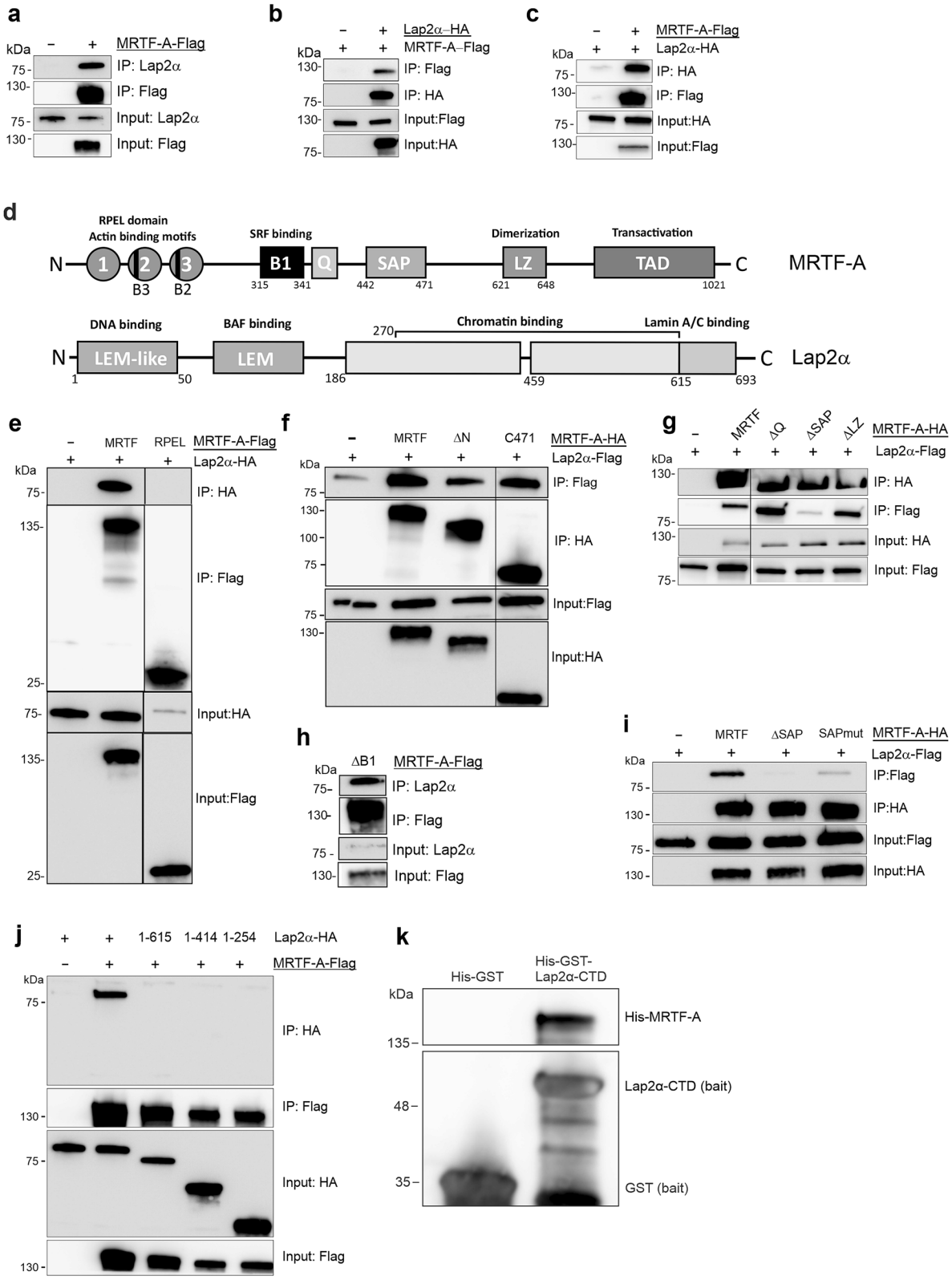
a
kDa
MRTF-A-Flag
IP: Lap2α
IP: Flag
Input: Lap2α
Input: Flag
b
Lap2α–HA
MRTF-A–Flag
IP: Flag
IP: HA
Input:Flag
Input:HA
c
MRTF-A-Flag
Lap2α-HA
IP: HA
IP: Flag
Input:HA
Input:Flag
d
RPEL domain
Actin binding motifs
SRF binding
Dimerization
Transactivation
N
C
MRTF-A
B3
B2
B1
Q
SAP
LZ
TAD
DNA binding
BAF binding
Chromatin binding
Lamin A/C binding
LEM-like
LEM
Lap2α
e
MRTF
RPEL
MRTF-A-Flag
Lap2α-HA
IP: HA
IP: Flag
Input:HA
Input:Flag
f
MRTF
ΔN
C471
MRTF-A-HA
Lap2α-Flag
IP: Flag
IP: HA
Input:Flag
Input:HA
g
MRTF
ΔQ
ΔSAP
ΔLZ
MRTF-A-HA
Lap2α-Flag
IP: HA
IP: Flag
Input: HA
Input: Flag
h
ΔB1
MRTF-A-Flag
IP: Lap2α
IP: Flag
Input: Lap2α
Input: Flag
i
MRTF
ΔSAP
SAPmut
MRTF-A-HA
Lap2α-Flag
IP:Flag
IP:HA
Input:Flag
Input:HA
j
1-615
1-414
1-254
Lap2α-HA
MRTF-A-Flag
IP: HA
IP: Flag
Input: HA
Input: Flag
k
His-GST
His-GST-Lap2α-CTD
His-MRTF-A
Lap2α-CTD (bait)
GST (bait)

◂**Figure 6.** MRTF-A binds to Lap2α. **(a)** Flag-tagged MRTF-A co-immunoprecipitates endogenous Lap2α. Transfected constructs are shown above the blots with the construct used as a bait underlined, protein weight markers on the left and the sample (immunoprecipitate or input) with the antibody used in Western Blot on the right. **(b)** HA-tagged Lap2α co-immunoprecipitates MRTF-A-Flag; data shown as in a. **(c)** Flag-tagged MRTF-A co-immunoprecipitates Lap2α-HA; data shown as in a. **(d)** Schematic presentation of MRTF-A and Lap2α domain structures. MRTF-A domains: 1,2,3—three RPEL motifs with two basic domains (B3 and B2); B1-basic domain responsible for SRF binding; Q-glutamine-rich domain; SAP-SAP (SAF A/B-Acinus-PIAS)-domain; *LZ* leucine-zipper domain; *TAD* transcription activation domain. Lap2α domains: LEM-like, LEM (Lap2-Emerin-MAN1 domain); chromatin binding domain; Lamin A/C binding domain. **(e)** Actin-binding RPEL domain of MRTF-A is not involved in the interaction with Lap2α; data shown as in a. Vertical line marks where cut was made. **(f)** N- and C-terminus of MRTF-A are not involved in the interaction with Lap2α; data shown as in a. Vertical line marks where cut was made. **(g)** Deletion of the SAP domain (ΔSAP), but not of the Q (ΔQ) and LZ (ΔLZ) domains MRTF-A reduces the interaction with Lap2α, data shown as in a. Vertical line marks where cut was made. **(h)** SRF-binding B1-domain of MRTF-A is not involved in the interaction with Lap2α. Data shown as in a. See also a for MRTF-A full-length protein for comparison. **(i)** Introducing point mutations into the SAP domain of MRTF-A impairs binding with Lap2α, data shown as in **(a)**. **(j)** Deleting the C-terminus of Lap2α impairs co-immunoprecipitation with MRTF-A, data shown as in **(a)**. **(k)** Pulldown assay of His-MRTF-A using His-GST-Lap2α-CTD (C-terminal domain) or His-GST as baits. All proteins were detected with anti-His antibody. See also supplementary S6.

muscle, and increased expression levels have been reported upon regeneration of skeletal muscle injuries[63], although decrease in MRTF-A levels are needed during myoblast fusion[64,65]. One mechanism to control MRTF-A abundance during myogenic differentiation is by microRNAs miR24-3p and miR-486-5p, which bind to the 3'UTR of the MRTF-A transcript and reduce MRTF-A expression[66]. Deregulation of MRTF-A/SRF pathway has been described in mice and cells expressing dilated cardiomyopathy (DCM)-causing lamin A/C mutations[13]. Interestingly, a mutation in Lap2α that lowers its affinity for lamin A/C has been identified in a family suffering from DCM[67]. It would be interesting to study whether MRTF-A/SRF target gene expression would be affected also in this DCM context. Further studies are needed to elucidate the functional significance of MRTF-A-mediated transcription to the multiple phenotypes associated with loss of Lap2α, and its potential significance to diseases caused by mutations in either Lap2α or lamin A/C. It will also be important to validate the role of Lap2α in regulating the other MRTF family members, MRTF-B and myocardin.

While the loss of Lap2α led to decreased binding of MRTF-A to the SRF target genes, our ChIP-seq data surprisingly revealed a higher number of MRTF-A peaks in the Lap2α KO cells compared to WT cells in starved conditions (Supplementary Fig. S4a). This result might be explained by increased nuclear localization of MRTF-A in starved KO cells that we showed in our localization experiments (Fig. 3), and might reflect binding of MRTF-A to lower affinity binding sites on chromatin. Motif analysis revealed that MRTF-A peaks were enriched for motifs of other transcription factors, such as ZBTB33 (Supplementary Table S4). Further experiments are required to elucidate the role of MRTF-A in SRF-independent transcription, and its cooperation with other transcription factors. Here it is also interesting to note that our co-immunoprecipitation experiments demonstrated the requirement for the MRTF-A SAP-domain in binding to Lap2α (Fig. 6i). The role of the SAP domain in MRTF-A function is still somewhat elusive. Its structure points to a possible interaction with DNA similarly to other SAP-domain containing proteins[68] and at least a set of specific genes associated with breast cancer have been suggested to be regulated by the MRTF SAP-domain, in SRF-independent manner[41]. Whether the interaction with Lap2α plays a role here awaits further studies.

Taken together, our research describes a novel mechanism to regulate the expression of MRTF-A/SRF target genes by Lap2α. In the future, it will be interesting to study further the biological relevance of this regulatory interaction in the context of both normal development and disease, and to explore the molecular mechanisms involved.

Material and methods

Plasmids. Details of the plasmid cloned for the study are available on request.

Plasmids used in the study: MRTF-A-GFP-N3, MRTF-A-2HA-N3, MRTF-A-2Flag-N3, MRTF-A-C471[4], MRTF-A-ΔN-2HA-N3 (amino acids 170–1021), MRTF-A-ΔQ-2HA-N3, MRTF-A-ΔSAP-2HA-N3, MRTF-A SAPmut, MRTF-A-ΔLZ-2HA-N3, RPEL-2HA-N3 (amino acids 1–204), MRTF-A-pDest10, Lap2α-2HA-C1, Lap2α-2Flag-C1, pET41a-3CΔ-Lap2α-CTD (amino acids 459–693), reporter plasmids were p3DA.luc[69], pRL-TK (Promega). For the design of MRTF-A SAPmut, we first analyzed the structure of MRTF-A SAP domain using Phyre^2 web portal[70]. Using structure of MRTF-A SAP domain (https://www.rcsb.org/structure/2KVU) as a reference, Phyre^2 identified several SAP domain-containing proteins, and we chose three of them characterized by high confidence (>98%) and high sequence identity (47–100%) of their SAP domains: ERI1 (human), SIZ1 (rice), THO1 (yeast). We did alignment of amino acid sequences and compared it with the data from Aravind and Koonin[68], who have described SAP domain as a putative DNA-binding motif. Although the most conserved residues were represented by five leucines, we decided not to mutate them because they are required to maintain correct folding of SAP domain helixes. We chose four amino acid residues, which appeared the most conserved among charged residues in SAP domains of analyzed proteins and replaced them with non-charged serine (K451S, R457S, K465S and R471S) in MRTF-A.

Name	Company/source	Application
RNA polymerase II CTD	Abcam ab 5408	ChIP-seq
MRTF-A	home-made rabbit antiserum provided by G.Posern (Martin Luther University Halle-Wittenberg)	ChIP-seq
Lap2α	mouse monoclonal antibody provided by R. Foisner (Max F. Perutz Laboratories)	ChIP-seq, IP
SRF	Cell Signaling Rabbit mAB #5147	ChIP-seq, WB
IGG	Santa Cruz sc-2027	ChIP-seq
MRTF-A	Santa Cruz G-8 sc-390324 1:50	IF
Alexa-Fluor-488-conjugated anti-mouse	Invitrogen A21155 1:500	IF
Alexa-Fluor-488-conjugated anti-rabbit	Invitrogen A11008 1:500	IF
HRP-conjugated Flag M2	Merck A8592 1:10,000	WB
HRP-conjugated HA	Merck H6533 1:7500	WB
Lap2α	Immuquest IQ175 1:2000	WB
Lap2	Abcam ab 185718 1:1000	WB
Lamin A/C	Cell Signaling Mouse mAb #4777	WB
BANF1/BAF	Abcam ab129184	WB
IGG	Abcam ab46540	IP
HRP-conjugated His	Merck A7058 1:5000	Pull-down

Table 1. List of antibodies used in the study.

Cell lines and transfections. NIH 3T3 cell line were obtained from the Treisman lab. Tetracycline-inducible MRTF-A-GFP-expressing NIH 3T3 cell line (R332) is described earlier[10]. Mouse dermal fibroblast (MDF) cell line with knock-out of Lap2α and the corresponding wild type MDF cell line were derived from Lap2α knockout mice[26]. All cell lines were cultured in Dulbecco's modified Eagle's medium (DMEM, Lonza) supplemented with 10% Fetal Bovine Serum (FBS; GIBCO), 100 units/ml Penicillin and 0.1 mg/ml Streptomycin (Thermo Fisher Scientific) and maintained in humidified 95% air/5% CO_2 incubator at + 37 °C. In addition, the R332 cell line was supplemented with 5 µg/ml Blasticidin (Invivogen) and 250 µg/ml Zeocin (Invivogen). Tetracycline (1 µg/ml) was added to the growth medium to induce the expression of MRTF-A-GFP.

For siRNA transfections, NIH 3T3 cells were plated onto 6-well tissue culture plate at a density of 25,000 cells per well one day prior to transfection. On the next day, cells were transfected with 20 nmol siRNA (mouse Lap2: 5'-GAUGUGACAGAGCUCUCUA predesigned from Sigma; mouse Lap2α: 5'-AGUCCAGCUAUCAAGAUUC; mouse Lap2β: 5'—GAGUACUCCCAUAGCUGAA; negative control: AllStars negative control from Qiagen) using Interferin transfection reagent (Polyplus transfection) according to manufacturer's protocol. On day 4, cells were re-transfected with siRNAs and DNA constructs if needed (for the Luciferase assay, see below), and the following day processed for western blotting, RNA extraction or luciferase assay.

For Western blotting analysis, cells were washed with 1 × PBS and lysed in 1 × Laemmli buffer. For RNA extraction and RT-qPCR analysis, re-transfected cells maintained in low-serum (0.3% FBS) DMEM for 24 h. After starvation, cells were stimulated with serum (15%) for 45 min and harvested for RNA extraction.

Luciferase assay. MDF or NIH cells were plated onto a 24-well plate. Next day MDF cells were transfected with SRF reporter p3D-Aluc (8 ng) and reference reporter pTK-RL (20 ng), with or without normalization control SRF-VP16 (20 ng) by using JetPrime transfection reagent. NIH cells were first transfected with siRNA as above, on day 4, re-transfected with p3DA.luc and pTK-RL plasmids. Cells were maintained in DMEM containing 0.3% FBS for 24 h and stimulated with serum (15%). After 7 h of stimulation, cells were harvested and analysed with the Dual-Luciferase reporter assay system (Promega) and a Multimode Plate Reader EnSpire (PerkinElmer), according to manufacturer's instructions. For data analysis, the activity of firefly luciferase was normalized to the renilla luciferase activity and SRF-VP16 was set to 100.

Immunostaining and microscopy. For microscopy, cells on coverslips were fixed with 4% paraformaldehyde for 15 min, washed four times with PBS and permeabilized for 5 min with 0.5% Triton X-100 (Merck) in PBS. For antibody staining, permeabilized cells were blocked with a blocking buffer (1% BSA, 1% Gelatin, 10% FBS) for 30 min and incubated with primary antibody for 1 h at RT (Table 1). Coverslips were washed three times with PBS and incubated with Alexa Fluor-conjugated secondary antibody for 1 h with or without DAPI (4',6-diamidino-2-phenylindole). Coverslips were washed three times with PBS and mounted in Mowiol 4-88 (Merck). Wide-field fluorescence microscope Leica (Leica, Welzlar, Germany) DM6000 with HCXPL APO 63x/1.40–0.60 oil objective and confocal Zeiss LSM700, 63x/1.3 objective and ZEN software were used to image the samples. The image files were processed with MIB software[71].

RNA seq. For RNA seq, NIH 3T3 cells were plated onto 10 cm plates. The following day, cells were transfected with siRNA as above (Lap2: 5'-GAUGUGACAGAGCUCUCUA from Sigma; negative control: AllStars negative control from Qiagen). Total RNA was extracted with a Nucleospin RNA kit from Macherey–Nagel according to the manufacturer's protocol from triplicates of control and Lap2-depleted samples. Libraries were

prepared for Illumina NextSeq 500 using Ribo-Zero rRNA Removal Kit (Illumina) and the NEBNext Ultra Directional RNA Library Prep at the Biomedicum Functional Genomics Unit (FuGU) according to the manufacturer's protocols. RNA-seq data sets were aligned using TopHat2[72] (using Chipster software[73]) to version mm10 of the mouse genome with the default settings. Counting aligned reads per genes were performed with HTSeq[74]. Differential expression analysis was performed with DESeq[75]. List of the transcribed genes was based on the aligned reads count cutoff > 1 from the RNA-Seq data from control vs Lap2-depleted NIH 3T3 cells. Gene ontology was performed using DAVID[76,77].

ChIP-seq. For chromatin immunoprecipitation (ChIP), NIH 3T3 or MDF cells were grown on 15 cm plates. Confluent cells (5×10^6 cells) were fixed in 1% paraformaldehyde/PBS for 10 min at RT, crosslinking was stopped by adding cold glycine to a final concentration of 0.125 M for 5 min, followed by harvesting in 500 ml of ice-cold PBS and spinning at 1000 *g* for 5 min at + 4 °C. Cell pellets were lysed in 300 µl of RIPA buffer and sonicated with Bioruptor (Diagenode; number of cycles = 15, power = HIGH, ON = 30 s, OFF = 30 s). IPs were carried out with 5 µg antibody (Table 1) overnight at 4 °C in a rotating wheel. The immuno-complexes were collected with 50 µl of protein A sepharose (17–0780-01, GE Healthcare) at 4 °C for two hours with rotation. The beads were pelleted by centrifugation at 4 °C for 1 min at 500 g and washed sequentially for 5 min on rotation with 1 ml of the following buffers: low-salt wash buffer (RIPA) (10 mM Tris–HCl (pH 8.0), 0.1% SDS, 1% Triton X-100, 1 mM EDTA, 140 mM NaCl, 0.1% sodium deoxycholate), high-salt wash buffer (10 mM Tris–HCl (pH 8.1), 0.1% SDS, 1% Triton X100, 1 mM EDTA, 500 mM NaCl, 0.1% sodium deoxycholate) and LiCl wash buffer (10 mM Tris–HCl (pH 8.1), 0.25 mM LiCl, 0.5% IGEPAL CA-630, 0.5% sodium deoxycholate, 1 mM EDTA). Finally, the beads were washed twice with 1 ml of TE buffer (10 mM Tris–HCl (pH 8.0), 1 mM EDTA). Chromatin was eluted in 150 µl of 1% SDS in TE buffer. The cross-linking was reversed by adding NaCl to final concentration of 200 mM and incubating at 65 °C overnight. The eluate was treated with Proteinase K and the DNA was recovered by extraction with phenol/chloroform/isoamyl alcohol (25/24/1, by vol.) and precipitated with 0.1 volume of 3 M sodium acetate (pH 5.2) and two volumes of ethanol using glycogen as a carrier. ChIP libraries were prepared for Illumina NextSeq 500 using NEBNext ChIP-Seq DNA Sample Prep Master Mix Set for Illumina (NEB E6240) and NEBNext® Multiplex Oligos for Illumina® (Index Primers Set 1) (NEB E7335) according to the manufacturer's protocols. Sequencing was performed with NextSeq500 at Biomedicum Functional Genomics Unit (FuGU). ChIP-Seq data sets were aligned using Bowtie2 (using Chipster software[73]) to version mm10 of the mouse genome with the default settings. Peak calling was performed with MASC2 against input[78]. To visualize and present ChIPseq data, we used Integrative Genomics Viewer, IGV[79] and EaSeq[80] (http://easeq.net). Heatmaps normalized on the input signal and plots showing average normalized fragment signal in the regions of interest were generated using EaSeq. The signal from the regions of interest were quantified with normalization per million per kilobase and statistically analyzed with Mann–Whitney U test using Origin. We used MEME-ChIP to perform comprehensive motif analysis (including motif discovery)[81].

Data access. ChIP-seq and RNA-seq data are available under Gene Expression Omnibus accession number GSE159371.

Single cell tracking assay. MDF cells were plated in 12-well plate (3000–4000 cells/well) in 10% FBS DMEM. On the next day, medium was replaced to 0.3% FBS DMEM, and cells were maintained under starved conditions for 24 h. After starvation, cells were stimulated with serum (15%) and immediately transferred into Cell-IQ Fluorescence imaging system (Chip-Man Technology) and monitored for 16 h at + 37 °C and CO_2 flow 25–30 mL/min. The images were taken with 20 min intervals. Images were stitched using wound healing assay tool of MIB software[71]; the stitched images were downsampled two times and saved as 3D-TIF stacks. The cell tracking was done using TrackMate plugin of Fiji[82]. Mitotic cells were identified and tracing of daughter cells started immediately after cell division. Each daughter cell was traced independently. The average speed of each cell was calculated and the results for all cells were plotted using violin plot function[83] in Matlab (Mathworks Inc, MA).

Co-IP assays. *For tagged proteins.* NIH 3T3 cells (1×10^6) were plated on 10 cm dishes and transfected with the appropriate HA/FLAG-tagged constructs (3 µg each plasmid) using Jet Prime transfection reagent. Twenty-four hours later, cells were harvested in IP buffer (0.5% Triton X-100, 50 mM Tris–HCl pH 7.5, 150 mM NaCl, protease inhibitor cocktail (Sigma-Aldrich)) and the lysates were cleared by centrifugation. Cleared lysates were then subjected to EZview Red Anti-HA Affinity Gel or Anti-FLAG M2 Affinity Gel (Sigma-Aldrich), incubated 3 h on rotation at + 4 °C and washed three times with IP buffer without Triton X-100. Bound proteins were eluted with 1 × SDS–PAGE loading buffer, boiled for 5 min, separated in 4–20% SDS–PAGE (BioRad) and electroblotted to nitrocellulose membrane. The membrane was probed with indicated antibodies (Table 1) diluted in 5% w/v non-fat dry milk or 2.5% BSA in PBS 0.1% Tween. Immunoreactive signals were acquired using WesternBright™ ECL-spray (Advansta).

For endogenous proteins. NIH 3T3 cells were plated on 15 cm dishes. When cell confluency reached 70–80%, cells were washed with ice-cold PBS and harvested in IP buffer (as described above).Cleared cell lysates were incubated with antibody (Lap2α or IgG, Table 1) for 4 h on rotation at + 4 °C, then bound antibody was precipitated with Dynabeads Protein G (Thermo Fisher Scientific). Washing and elution was done according the protocol for Dynabeads Protein G (Thermo Fisher Scientific). All original western blots are available in Supplementary 7; note that some blots were cut to detect several different proteins from the same blot.

Real-time quantitative PCR. NIH or MDF cells were plated on 35 mm dishes. On the next day, the media was changed to fresh growth media containing 0.3% FBS. Cells were maintained in low-serum conditions for 24 h. On day 3, cells were stimulated with 15% FBS for 45 min and total RNA was extracted using Nucleospin RNA II kit according to the manufacturer's protocol (Macherey–Nagel). Five hundred micrograms of total RNA was used for complementary DNA synthesis using Thermo Scientific RT–PCR kit (Thermo Scientific). Quantitative PCR was carried out using the Bio-Rad CFX machine (Bio-Rad) and SYBR green qPCR reagent (Thermo Scientific). Gene specific primers are listed below:

Gapdh_fw: 5′-TGCACCACCAACTGCTTAGC-3′
Gapdh_rev: 5′-GGCATGGACTGTGGTCATGAG-3′
Acta2 fw: 5′-ACTGGGACGACATGGAAAAG-3′
Acta2 rev: 5′-GTTCAGTGGTGCCTCTGTCA-3′
Vcl fw: 5′-CTTTGTGCAGGCAAGGAACG-3′
Vcl rev: 5′-GCTGCATTCTCCACTTTGGC-3′
Tagln fw: 5'-CTATGAAGGTAAGGATATGGC
Tagln rev: 5'-TCTGTGAAGTCCCTCTTATG
Egr1 fw: 5'-CAGAGTCCTTTTCTGACATC
Egr1 rev: 5'-GAGAAGCGGCCAGTATAG
Egr3 fw: 5'-CCACCTCACCACTCACATCC
Egr3 rev: 5'-CTTGAGGTGGATCTTGGCGT
Fos fw: 5'-TACTACCATTCCCCAGCCGA
Fos rev: 5'-GCTGTCACCGTGGGGATAAA.

Relative expression levels were calculated by the comparative C_T method, normalizing to the Gapdh cDNA: $2^{-C}{}_T$ (target)/$2^{-C}{}_T$ (Gapdh).

Expression and purification of MRTF-A protein. Recombinant mouse His-MRTF-A was expressed by using MultiBac baculovirus expression system. MRTF-A-pDest10 plasmid was transformed into DH10MultiBac cells, recombinant bacmids were prepared and the presence of the correct construct verified by PCR. The verified bacmid was transfected into Sf21 cells using Fugene HD transfection reagent (Promega). The obtained viral stock was amplified and used for protein expression. The expression of His-MRTF-A was done by infecting cells at the density of 2.0×10^6 cells/ml with the baculoviral stock at a multiplicity of infection (MOI) of 1. The cells were collected after 96 h and the pellets were snap frozen and stored at −80 °C. The expression was verified by Western blot. For purification, the cell pellets were resuspended in lysis buffer (25 mM Tris–HCl pH 8.0, 10 mM NaCl, 1 mM $MgCl_2$, 2 mM B-mercaptoethanol, 0.2% Igepal) with protease inhibitors (Roche) and benzonase nuclease (1 µl of 250 units/µl, Sigma-Aldrich) and lysed with EmulsiFlex-C3 (AVESTIN) with gauge pressure ~ 15,000 psi for 10 min. Immediately after lysis, the NaCl concentration was adjusted to 200 mM and 10 mM imidazole was added. Cell extract was incubated for 10 min at + 4 °C and clarified by centrifugation at 39,000 *g* for 30 min and immediately processed to metal (Ni^{2+}) affinity purification using Ni^{2+}-NTA agarose beads (Qiagen) equilibrated with lysis buffer. Beads were incubated with extract for 2 h on rotation at + 4 °C and washed three times with buffer A (25 mM Tris–HCl pH 8.0, 300 mM NaCl, 2 mM B-mercaptoethanol) and two times with buffer A with addition of 20 mM imidazole. The last wash was conducted in a disposable 10 ml Poly-prep column (Bio-RAD) and the protein was eluted from the beads with elution buffer (25 mM Tris–HCl pH 8.0, 100 mM NaCl, 500 mM imidazole). The protein was further purified with gel filtration column Superdex 200 HiLoad 16/60 (Pharmacia), which was equilibrated with buffer B (50 mM Tris–HCl pH 8.0, 100 mM NaCl, 1 mM DTT, 0.5 mM EDTA, 10% glycerol). Fractions were analyzed by SDS-PAGE and those containing His-MRTF-A were concentrated and stored at −80 °C.

Expression of Lap2α-CTD. The coding region corresponding to murine Lap2α residues 459–693 was cloned to pET 4.1-3CD. *E.coli* cells expressing His-GST-Lap2α-CTD were grown at 37 °C for 2–3 h until OD_{600} reached 0.6–1.0 and then induced with IPTG to a final concentration of 1 mM. Then cells were cultivated for 3 h at 37 °C, harvested by centrifugation at 4000 rpm 3 min, frozen and stored at −80 °C.

Pull-down assay. His-GST (10 µl) and His-GST-Lap2α-CTD (100 µl) *E.coli* lysates were immobilized on 50 µl of Protino 4B glutathione agarose (Macherey–Nagel) equilibrated with binding buffer 1 (25 mM Tris–HCl pH 7.5, 150 mM NaCl, 1 mM DTT) in a total reaction volume of 300 µl in binding buffer 1 for 2 h on rotation at + 4 °C. Beads were washed once with binding buffer 1, three times with binding buffer 2 (25 mM Tris–HCl pH 7.5, 500 mM NaCl, 1 mM DTT) and once with binding buffer 1. After the washes, beads were incubated with 1.5 µM purified recombinant His-MRTF-A in binding buffer 1 for overnight on rotation at + 4 °C. After incubation the beads were washed three times with binding buffer 1 and bound proteins were eluted with 1xSDS-PAGE loading buffer. Samples were boiled for 5 min and the proteins were separated in 4–20% Mini-PROTEAN TGX Precast Protein Gel (Bio-RAD) and electroblotted to nitrocellulose membrane. The membrane was probed with anti-His antibody to assess the association of His-MRTF-A with GST-fusions (Table 1). Western blotting detection system was WesternBright™ ECL-spray (Advansta).

Statistical analysis. Statistical analyses were performed in Excel or XLSTAT by two-tailed Student's *t*-test, with two-sample unequal variance for the data conformed to normal distribution (SRF reporter activity, expression of SRF target genes, MRTF-A localization). Non-parametric Kolmogorov–Smirnov test, with the significance level of 0.05, was applied to Single cell tracking assay data, because the data did not conform to normal distribution.

Received: 25 August 2021; Accepted: 18 January 2022
Published online: 10 February 2022

References

1. Lambert, S. A. *et al.* The human transcription factors. *Cell* **175**, 598–599. https://doi.org/10.1016/j.cell.2018.09.045 (2018).
2. Lee, S. M., Vasishtha, M. & Prywes, R. Activation and repression of cellular immediate early genes by serum response factor cofactors. *J. Biol. Chem.* **285**, 22036–22049. https://doi.org/10.1074/jbc.M110.108878 (2010).
3. Miano, J. M., Long, X. & Fujiwara, K. Serum response factor: Master regulator of the actin cytoskeleton and contractile apparatus. *Am. J. Physiol. Cell Physiol.* **292**, C70-81. https://doi.org/10.1152/ajpcell.00386.2006 (2007).
4. Miralles, F., Posern, G., Zaromytidou, A. I. & Treisman, R. Actin dynamics control SRF activity by regulation of its coactivator MAL. *Cell* **113**, 329–342. https://doi.org/10.1016/s0092-8674(03)00278-2 (2003).
5. Zaromytidou, A. I., Miralles, F. & Treisman, R. MAL and ternary complex factor use different mechanisms to contact a common surface on the serum response factor DNA-binding domain. *Mol. Cell Biol.* **26**, 4134–4148. https://doi.org/10.1128/MCB.01902-05 (2006).
6. Buchwalter, G., Gross, C. & Wasylyk, B. Ets ternary complex transcription factors. *Gene* **324**, 1–14. https://doi.org/10.1016/j.gene.2003.09.028 (2004).
7. Olson, E. N. & Nordheim, A. Linking actin dynamics and gene transcription to drive cellular motile functions. *Nat. Rev. Mol. Cell Biol.* **11**, 353–365. https://doi.org/10.1038/nrm2890 (2010).
8. Mouilleron, S., Langer, C. A., Guettler, S., McDonald, N. Q. & Treisman, R. Structure of a pentavalent G-actin*MRTF-A complex reveals how G-actin controls nucleocytoplasmic shuttling of a transcriptional coactivator. *Sci Signal* **4**, ra40. https://doi.org/10.1126/scisignal.2001750 (2011).
9. Pawlowski, R., Rajakyla, E. K., Vartiainen, M. K. & Treisman, R. An actin-regulated importin alpha/beta-dependent extended bipartite NLS directs nuclear import of MRTF-A. *EMBO J.* **29**, 3448–3458. https://doi.org/10.1038/emboj.2010.216 (2010).
10. Vartiainen, M. K., Guettler, S., Larijani, B. & Treisman, R. Nuclear actin regulates dynamic subcellular localization and activity of the SRF cofactor MAL. *Science* **316**, 1749–1752. https://doi.org/10.1126/science.1141084 (2007).
11. Baarlink, C., Wang, H. & Grosse, R. Nuclear actin network assembly by formins regulates the SRF coactivator MAL. *Science* **340**, 864–867. https://doi.org/10.1126/science.1235038 (2013).
12. Wang, Y. *et al.* GPCR-induced calcium transients trigger nuclear actin assembly for chromatin dynamics. *Nat. Commun.* **10**, 5271. https://doi.org/10.1038/s41467-019-13322-y (2019).
13. Ho, C. Y., Jaalouk, D. E., Vartiainen, M. K. & Lammerding, J. Lamin A/C and emerin regulate MKL1-SRF activity by modulating actin dynamics. *Nature* **497**, 507–511. https://doi.org/10.1038/nature12105 (2013).
14. Holaska, J. M., Kowalski, A. K. & Wilson, K. L. Emerin caps the pointed end of actin filaments: Evidence for an actin cortical network at the nuclear inner membrane. *PLoS Biol.* **2**, E231. https://doi.org/10.1371/journal.pbio.0020231 (2004).
15. Willer, M. K. & Carroll, C. W. Substrate stiffness-dependent regulation of the SRF-Mkl1 co-activator complex requires the inner nuclear membrane protein Emerin. *J. Cell Sci.* **130**, 2111–2118. https://doi.org/10.1242/jcs.197517 (2017).
16. Plessner, M., Melak, M., Chinchilla, P., Baarlink, C. & Grosse, R. Nuclear F-actin formation and reorganization upon cell spreading. *J. Biol. Chem.* **290**, 11209–11216. https://doi.org/10.1074/jbc.M114.627166 (2015).
17. Thakar, K., May, C. K., Rogers, A. & Carroll, C. W. Opposing roles for distinct LINC complexes in regulation of the small GTPase RhoA. *Mol. Biol. Cell* **28**, 182–191. https://doi.org/10.1091/mbc.E16-06-0467 (2017).
18. Berger, R. *et al.* The characterization and localization of the mouse thymopoietin/lamina-associated polypeptide 2 gene and its alternatively spliced products. *Genome Res.* **6**, 361–370. https://doi.org/10.1101/gr.6.5.361 (1996).
19. Harris, C. A. *et al.* Structure and mapping of the human thymopoietin (TMPO) gene and relationship of human TMPO beta to rat lamin-associated polypeptide 2. *Genomics* **28**, 198–205. https://doi.org/10.1006/geno.1995.1131 (1995).
20. Foisner, R. & Gerace, L. Integral membrane proteins of the nuclear envelope interact with lamins and chromosomes, and binding is modulated by mitotic phosphorylation. *Cell* **73**, 1267–1279. https://doi.org/10.1016/0092-8674(93)90355-t (1993).
21. Lang, C. & Krohne, G. Lamina-associated polypeptide 2beta (LAP2beta) is contained in a protein complex together with A- and B-type lamins. *Eur. J. Cell Biol.* **82**, 143–153. https://doi.org/10.1078/0171-9335-00305 (2003).
22. Dechat, T. *et al.* Lamina-associated polypeptide 2alpha binds intranuclear A-type lamins. *J. Cell Sci.* **113**(Pt 19), 3473–3484 (2000).
23. Prufert, K., Winkler, C., Paulin-Levasseur, M. & Krohne, G. The lamina-associated polypeptide 2 (LAP2) genes of zebrafish and chicken: No LAP2alpha isoform is synthesised by non-mammalian vertebrates. *Eur. J. Cell Biol.* **83**, 403–411. https://doi.org/10.1078/0171-9335-00402 (2004).
24. Dechat, T. *et al.* Detergent-salt resistance of LAP2alpha in interphase nuclei and phosphorylation-dependent association with chromosomes early in nuclear assembly implies functions in nuclear structure dynamics. *EMBO J.* **17**, 4887–4902. https://doi.org/10.1093/emboj/17.16.4887 (1998).
25. Dechat, T., Vlcek, S. & Foisner, R. Review: Lamina-associated polypeptide 2 isoforms and related proteins in cell cycle-dependent nuclear structure dynamics. *J. Struct. Biol.* **129**, 335–345. https://doi.org/10.1006/jsbi.2000.4212 (2000).
26. Naetar, N. *et al.* Loss of nucleoplasmic LAP2alpha-lamin A complexes causes erythroid and epidermal progenitor hyperproliferation. *Nat. Cell Biol.* **10**, 1341–1348. https://doi.org/10.1038/ncb1793 (2008).
27. Cohen, T. V. *et al.* Defective skeletal muscle growth in lamin A/C-deficient mice is rescued by loss of Lap2alpha. *Hum. Mol. Genet.* **22**, 2852–2869. https://doi.org/10.1093/hmg/ddt135 (2013).
28. Gesson, K. *et al.* A-type lamins bind both hetero- and euchromatin, the latter being regulated by lamina-associated polypeptide 2 alpha. *Genome Res.* **26**, 462–473. https://doi.org/10.1101/gr.196220.115 (2016).
29. Dorner, D. *et al.* Lamina-associated polypeptide 2alpha regulates cell cycle progression and differentiation via the retinoblastoma-E2F pathway. *J. Cell Biol.* **173**, 83–93. https://doi.org/10.1083/jcb.200511149 (2006).
30. Tang, Y., Zhang, X., Ge, W. & Zhou, Y. Knockdown of LAP2alpha inhibits osteogenic differentiation of human adipose-derived stem cells by activating NF-kappaB. *Stem Cell Res. Ther.* **11**, 263. https://doi.org/10.1186/s13287-020-01774-9 (2020).
31. Gotic, I. *et al.* Lamina-associated polypeptide 2alpha loss impairs heart function and stress response in mice. *Circ. Res.* **106**, 346–353. https://doi.org/10.1161/CIRCRESAHA.109.205724 (2010).
32. Mirza, A. N. *et al.* LAP2 proteins chaperone GLI1 movement between the lamina and chromatin to regulate transcription. *Cell* **176**, 198-212e115. https://doi.org/10.1016/j.cell.2018.10.054 (2019).

33. Kircher, P. *et al.* Filamin A interacts with the coactivator MKL1 to promote the activity of the transcription factor SRF and cell migration. *Sci Signal* **8**, ra112. https://doi.org/10.1126/scisignal.aad2959 (2015).
34. Rajakyla, E. K. *et al.* RNA export factor Ddx19 is required for nuclear import of the SRF coactivator MKL1. *Nat. Commun.* **6**, 5978. https://doi.org/10.1038/ncomms6978 (2015).
35. Morita, T., Mayanagi, T. & Sobue, K. Reorganization of the actin cytoskeleton via transcriptional regulation of cytoskeletal/focal adhesion genes by myocardin-related transcription factors (MRTFs/MAL/MKLs). *Exp. Cell Res.* **313**, 3432–3445. https://doi.org/10.1016/j.yexcr.2007.07.008 (2007).
36. Gualdrini, F. *et al.* SRF co-factors control the balance between cell proliferation and contractility. *Mol. Cell* **64**, 1048–1061. https://doi.org/10.1016/j.molcel.2016.10.016 (2016).
37. Leitner, L. *et al.* MAL/MRTF-A controls migration of non-invasive cells by upregulation of cytoskeleton-associated proteins. *J. Cell Sci.* **124**, 4318–4331. https://doi.org/10.1242/jcs.092791 (2011).
38. Medjkane, S., Perez-Sanchez, C., Gaggioli, C., Sahai, E. & Treisman, R. Myocardin-related transcription factors and SRF are required for cytoskeletal dynamics and experimental metastasis. *Nat. Cell Biol.* **11**, 257–268. https://doi.org/10.1038/ncb1833 (2009).
39. Pipes, G. C., Creemers, E. E. & Olson, E. N. The myocardin family of transcriptional coactivators: Versatile regulators of cell growth, migration, and myogenesis. *Genes Dev.* **20**, 1545–1556. https://doi.org/10.1101/gad.1428006 (2006).
40. Fornerod, M., Ohno, M., Yoshida, M. & Mattaj, I. W. CRM1 is an export receptor for leucine-rich nuclear export signals. *Cell* **90**, 1051–1060. https://doi.org/10.1016/s0092-8674(00)80371-2 (1997).
41. Gurbuz, I., Ferralli, J., Roloff, T., Chiquet-Ehrismann, R. & Asparuhova, M. B. SAP domain-dependent Mkl1 signaling stimulates proliferation and cell migration by induction of a distinct gene set indicative of poor prognosis in breast cancer patients. *Mol. Cancer* **13**, 22. https://doi.org/10.1186/1476-4598-13-22 (2014).
42. Guettler, S., Vartiainen, M. K., Miralles, F., Larijani, B. & Treisman, R. RPEL motifs link the serum response factor cofactor MAL but not myocardin to Rho signaling via actin binding. *Mol. Cell Biol.* **28**, 732–742. https://doi.org/10.1128/MCB.01623-07 (2008).
43. Vlcek, S., Just, H., Dechat, T. & Foisner, R. Functional diversity of LAP2alpha and LAP2beta in postmitotic chromosome association is caused by an alpha-specific nuclear targeting domain. *EMBO J.* **18**, 6370–6384. https://doi.org/10.1093/emboj/18.22.6370 (1999).
44. Mattout-Drubezki, A. & Gruenbaum, Y. Dynamic interactions of nuclear lamina proteins with chromatin and transcriptional machinery. *Cell Mol. Life Sci.* **60**, 2053–2063. https://doi.org/10.1007/s00018-003-3038-3 (2003).
45. Simon, D. N. & Wilson, K. L. The nucleoskeleton as a genome-associated dynamic "network of networks". *Nat. Rev. Mol. Cell Biol.* **12**, 695–708. https://doi.org/10.1038/nrm3207 (2011).
46. Nili, E. *et al.* Nuclear membrane protein LAP2beta mediates transcriptional repression alone and together with its binding partner GCL (germ-cell-less). *J. Cell Sci.* **114**, 3297–3307 (2001).
47. Somech, R. *et al.* The nuclear-envelope protein and transcriptional repressor LAP2beta interacts with HDAC3 at the nuclear periphery, and induces histone H4 deacetylation. *J. Cell Sci.* **118**, 4017–4025. https://doi.org/10.1242/jcs.02521 (2005).
48. Cai, M. *et al.* Solution structure of the constant region of nuclear envelope protein LAP2 reveals two LEM-domain structures: one binds BAF and the other binds DNA. *EMBO J.* **20**, 4399–4407. https://doi.org/10.1093/emboj/20.16.4399 (2001).
49. Laguri, C. *et al.* Structural characterization of the LEM motif common to three human inner nuclear membrane proteins. *Structure* **9**, 503–511. https://doi.org/10.1016/s0969-2126(01)00611-6 (2001).
50. Segura-Totten, M. & Wilson, K. L. BAF: Roles in chromatin, nuclear structure and retrovirus integration. *Trends Cell Biol.* **14**, 261–266. https://doi.org/10.1016/j.tcb.2004.03.004 (2004).
51. Vlcek, S., Korbei, B. & Foisner, R. Distinct functions of the unique C terminus of LAP2alpha in cell proliferation and nuclear assembly. *J. Biol. Chem.* **277**, 18898–18907. https://doi.org/10.1074/jbc.M200048200 (2002).
52. Treisman, R., Marais, R. & Wynne, J. Spatial flexibility in ternary complexes between SRF and its accessory proteins. *EMBO J.* **11**, 4631–4640 (1992).
53. Panayiotou, R. *et al.* Phosphorylation acts positively and negatively to regulate MRTF-A subcellular localisation and activity. *Elife* https://doi.org/10.7554/eLife.15460 (2016).
54. Nakagawa, K. & Kuzumaki, N. Transcriptional activity of megakaryoblastic leukemia 1 (MKL1) is repressed by SUMO modification. *Genes Cells* **10**, 835–850. https://doi.org/10.1111/j.1365-2443.2005.00880.x (2005).
55. Yang, Y., Li, Z., Guo, J. & Xu, Y. Deacetylation of MRTF-A by SIRT1 defies senescence induced down-regulation of collagen type I in fibroblast cells. *Biochim. Biophys. Acta Mol. Basis Dis.* **1866**, 165723. https://doi.org/10.1016/j.bbadis.2020.165723 (2020).
56. Yu, L., Li, Z., Fang, M. & Xu, Y. Acetylation of MKL1 by PCAF regulates pro-inflammatory transcription. *Biochim. Biophys. Acta Gene Regul. Mech.* **839–847**, 2017. https://doi.org/10.1016/j.bbagrm.2017.05.006 (1860).
57. Zhang, M. *et al.* HDAC6 regulates the MRTF-A/SRF axis and vascular smooth muscle cell plasticity. *JACC Basic Transl. Sci.* **3**, 782–795. https://doi.org/10.1016/j.jacbts.2018.08.010 (2018).
58. Gotic, I. *et al.* Loss of LAP2 alpha delays satellite cell differentiation and affects postnatal fiber-type determination. *Stem Cells* **28**, 480–488. https://doi.org/10.1002/stem.292 (2010).
59. Mack, C. P. & Hinson, J. S. Regulation of smooth muscle differentiation by the myocardin family of serum response factor co-factors. *J. Thromb. Haemost.* **3**, 1976–1984. https://doi.org/10.1111/j.1538-7836.2005.01316.x (2005).
60. Selvaraj, A. & Prywes, R. Megakaryoblastic leukemia-1/2, a transcriptional co-activator of serum response factor, is required for skeletal myogenic differentiation. *J. Biol. Chem.* **278**, 41977–41987. https://doi.org/10.1074/jbc.M305679200 (2003).
61. Parmacek, M. S. Myocardin-related transcription factors: Critical coactivators regulating cardiovascular development and adaptation. *Circ. Res.* **100**, 633–644. https://doi.org/10.1161/01.RES.0000259563.61091.e8 (2007).
62. Cenik, B. K. *et al.* Myocardin-related transcription factors are required for skeletal muscle development. *Development* **143**, 2853–2861. https://doi.org/10.1242/dev.135855 (2016).
63. Mokalled, M. H. & Poss, K. D. A regeneration toolkit. *Dev. Cell* **47**, 267–280. https://doi.org/10.1016/j.devcel.2018.10.015 (2018).
64. Charrasse, S. *et al.* RhoA GTPase regulates M-cadherin activity and myoblast fusion. *Mol. Biol. Cell* **17**, 749–759. https://doi.org/10.1091/mbc.e05-04-0284 (2006).
65. Iwasaki, K., Hayashi, K., Fujioka, T. & Sobue, K. Rho/Rho-associated kinase signal regulates myogenic differentiation via myocardin-related transcription factor-A/Smad-dependent transcription of the Id3 gene. *J. Biol. Chem.* **283**, 21230–21241. https://doi.org/10.1074/jbc.M710525200 (2008).
66. Holstein, I. *et al.* Post-transcriptional regulation of MRTF-A by miRNAs during myogenic differentiation of myoblasts. *Nucleic Acids Res.* **48**, 8927–8942. https://doi.org/10.1093/nar/gkaa596 (2020).
67. Taylor, M. R. *et al.* Thymopoietin (lamina-associated polypeptide 2) gene mutation associated with dilated cardiomyopathy. *Hum. Mutat.* **26**, 566–574. https://doi.org/10.1002/humu.20250 (2005).
68. Aravind, L. & Koonin, E. V. SAP—A putative DNA-binding motif involved in chromosomal organization. *Trends Biochem. Sci.* **25**, 112–114. https://doi.org/10.1016/s0968-0004(99)01537-6 (2000).
69. Geneste, O., Copeland, J. W. & Treisman, R. LIM kinase and Diaphanous cooperate to regulate serum response factor and actin dynamics. *J. Cell Biol.* **157**, 831–838. https://doi.org/10.1083/jcb.200203126 (2002).
70. Kelley, L. A., Mezulis, S., Yates, C. M., Wass, M. N. & Sternberg, M. J. The Phyre2 web portal for protein modeling, prediction and analysis. *Nat. Protoc.* **10**, 845–858. https://doi.org/10.1038/nprot.2015.053 (2015).
71. Belevich, I., Joensuu, M., Kumar, D., Vihinen, H. & Jokitalo, E. Microscopy image browser: A platform for segmentation and analysis of multidimensional datasets. *PLoS Biol.* **14**, e1002340. https://doi.org/10.1371/journal.pbio.1002340 (2016).

72. Kim, D. *et al.* TopHat2: Accurate alignment of transcriptomes in the presence of insertions, deletions and gene fusions. *Genome Biol.* **14**, R36. https://doi.org/10.1186/gb-2013-14-4-r36 (2013).
73. Kallio, M. A. *et al.* Chipster: User-friendly analysis software for microarray and other high-throughput data. *BMC Genomics* **12**, 507. https://doi.org/10.1186/1471-2164-12-507 (2011).
74. Anders, S., Pyl, P. T. & Huber, W. HTSeq–A Python framework to work with high-throughput sequencing data. *Bioinformatics* **31**, 166–169. https://doi.org/10.1093/bioinformatics/btu638 (2015).
75. Love, M. I., Huber, W. & Anders, S. Moderated estimation of fold change and dispersion for RNA-seq data with DESeq2. *Genome Biol* **15**, 550. https://doi.org/10.1186/s13059-014-0550-8 (2014).
76. da Huang, W., Sherman, B. T. & Lempicki, R. A. Systematic and integrative analysis of large gene lists using DAVID bioinformatics resources. *Nat. Protoc.* **4**, 44–57. https://doi.org/10.1038/nprot.2008.211 (2009).
77. da Huang, W., Sherman, B. T. & Lempicki, R. A. Bioinformatics enrichment tools: Paths toward the comprehensive functional analysis of large gene lists. *Nucleic Acids Res.* **37**, 1–13. https://doi.org/10.1093/nar/gkn923 (2009).
78. Zhang, Y. *et al.* Model-based analysis of ChIP-Seq (MACS). *Genome Biol.* **9**, R137. https://doi.org/10.1186/gb-2008-9-9-r137 (2008).
79. Robinson, J. T. *et al.* Integrative genomics viewer. *Nat. Biotechnol.* **29**, 24–26. https://doi.org/10.1038/nbt.1754 (2011).
80. Lerdrup, M., Johansen, J. V., Agrawal-Singh, S. & Hansen, K. An interactive environment for agile analysis and visualization of ChIP-sequencing data. *Nat. Struct. Mol. Biol.* **23**, 349–357. https://doi.org/10.1038/nsmb.3180 (2016).
81. Bailey, T. L. *et al.* MEME SUITE: Tools for motif discovery and searching. *Nucleic Acids Res.* **37**, W202-208. https://doi.org/10.1093/nar/gkp335 (2009).
82. Tinevez, J. Y. *et al.* TrackMate: An open and extensible platform for single-particle tracking. *Methods* **115**, 80–90. https://doi.org/10.1016/j.ymeth.2016.09.016 (2017).
83. Hoffmann, H. *Violin Plot*. https://se.mathworks.com/matlabcentral/fileexchange/45134-violin-plot (2015).

Acknowledgements

We thank Paula Maanselkä for excellent assistance. Imaging was performed at Light Microscopy Unit (LMU), which is supported by Helsinki Institute for Life Science (HiLIFE) and Biocenter Finland. This work was supported by grants (to MKV) from Sigrid Juselius foundation, Academy of Finland, Jane and Aatos Erkko foundation, Finnish Cancer foundation and HiLIFE.

Author contributions

E.S., M.S. and M.K.V. conceived and planed out the experiments. E.S., A.P. and S.K. performed the experiments. E.S. and M.S. analyzed the results. G.P. and R.F. provided reagents and intellectual input into the project. E.S., M.S. and M.K.V. wrote the manuscript based on input from G.P. and R.F. M.K.V. supervised and obtained funding for the project.

Competing interests

The authors declare no competing interests.

Additional information

Supplementary Information The online version contains supplementary material available at https://doi.org/10.1038/s41598-022-06135-5.

Correspondence and requests for materials should be addressed to M.K.V.

Reprints and permissions information is available at www.nature.com/reprints.

Publisher's note Springer Nature remains neutral with regard to jurisdictional claims in published maps and institutional affiliations.